Spectroscopic, Electrochemical, Magnetic and Structural Characterization of an Hexamethylenetetramine Co(II) Porphyrin Complex - Application in the Catalytic Degradation of Vat Yellow 1 Dye

Soumaya Nasri, Melek Hajji, Mouhieddinne Guergueb, Selma Dhifaoui, Valerie Marvaud, Frédérique Loiseau, Florian Molton, Thierry Roisnel, Taha Guerfel, Habib Nasri

Spectroscopic, Electrochemical, Magnetic and Structural Characterization of an Hexamethylenetetramine Co(II) Porphyrin Complex – Application in the Catalytic Degradation of Vat Yellow 1 dye

Soumaya Nasri[a,b,*], Melek Hajji[c], Mouhieddinne Guergueb[a], Selma Dhifaoui[a], Valérie Marvaud[d], Frédérique Loiseau[e], Florian Molton[e], Thierry Roisnel[f], Taha Guerfel[c], Habib Nasri[a]

[a] *Laboratory of Physico-chemistry of Materials, Faculty of Sciences of Monastir, University of Monastir, Avenue de l'environnement, 5019 Monastir, Tunisia*
[b] *Department of Chemistry, College of Science Al-Zulfi, Majmaah University, Saudi Arabia*
[c] *Research Unit: Electrochemistry, Materials and Environment, University of Kairouan, 3100, Kairouan, Tunisia*
[d] *IPCM, Institut Parisien de Chimie Moléculaire, UPMC, Sorbonne Université, Paris, Cedex 0, France*
[e] *Département de Chimie Moléculaire, 301 rue de la Chimie, Université Grenoble Alpes, CS 40700, 38058 Grenoble Cedex 9, France*
[f] *Centre de Diffractométrie X, Institut des Sciences Chimiques de Rennes, UMR 6226, CNRS-Université de Rennes 1, Campus de Beaulieu, 35042 Rennes Cedex, France*

ARTICLE INFO

Article history:
Received 17 September 2020
Revised 30 October 2020
Accepted 19 November 2020
Available online 28 November 2020

ABSTRACT

In this study, a new cobaltous-(hexamethylenetetramine) [*meso*-tetra(*para*-methoxyphenyl)porphyrin complex with the formula [Co^{II}(TMPP)(HMTA)] (**I**) was synthesized. The molecular structure was confirmed in solution by ^{1}H NMR spectroscopy and mass spectrometry methods, and the single crystal X-ray diffraction structure of (**I**) was determined at both room temperature and low temperature. This species was further characterized by infrared, UV-visible and fluorescence spectroscopies, magnetic susceptibility measurements and cyclic voltammetry. The chemical reactivity behavior was also assessed theoretically through Density Functional Theory (DFT) approach. Magnetic investigation indicates that the Co(II)-HMTA porphyrin (**I**) species at low temperature is a cobaltous low-spin (S = 1/2) species while at high temperature complex (**I**) exhibits a spin-crossover low-spin (S = 1/2) ↔ high-spin (S = 3/2). The adsorption kinetic of the "vat yellow 1 dye" was carried out in aqueous solution at pH = 6. The experimental results are better fitted using the pseudo second order model. Furthermore, complex (**I**) was tested as catalyst in the degradation of the vat yellow 1 dye using an aqueous H_2O_2 solution and by photodegradation under solar light.

1. Introduction

Cobaltous metalloporphyrins have been investigated since the sixties because of the biological importance of cobalamins which have a porphyrin-like structure and were used as models for hemoproteins and cobalamins especially the vitamin B12 [1-3]. Cobalt(II) metalloporphyrins with the 3d [7] electron configuration of the ground state, are known to be air stable and on the base of numerous [4] EPR studies it is known that the unpaired electron is located in the axial d_{z^2} orbital ($^2A_1$ state) [2,5]. These cobaltous species exist in the low-spin, square-planar configuration in noncoordinating solvents [6]. These tetracoordinated species have a high affinity for single nitrogenous cyclic axial ligands such as pyridine and imidazole leading to pentacoordinated cobaltous derivative type [Co^{II}(Porph)(L)] (Porph = porphyrinato, L = N-donor neutral cyclic axial ligand) and a lower affinity for binding a second ligand. In the literature, the major published cobaltous porphyrin complexes studies concern either tetracoordinate or pentacoodinate species [7-10]. Nevertheless, the molecular structures of few hexacoordinated Co(II) porphyrins are known, e.g. [Co^{II}(TPP)(amp)$_2$] (TPP: *meso*-tetraphenylporphyrinato and amp = 2-aminophenol) [11]. It is noteworthy that Co(II) porphyrins are increasingly used in several fields such as catalysis; e.g., the [Co^{II}(P1)] complex (P1 = the D_2-symmetric chiral porphyrin 3,5-Di^{t}Bu-ChenPhyrinas) which have been reported to be effective catalysts for the stereos-

* Corresponding author.
E-mail address: soumaya.n@mu.edu.sa (S. Nasri).

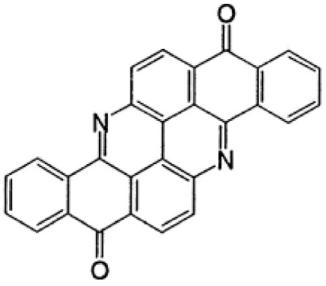

Scheme 1. Structure of the vat yellow 1 dye.

elective cyclopropanation of alkenes with unique reactivity profiles [12]. These compounds are also used in fuel cells, [13] as building blocks, [14] as antifungal and antibacterial drugs [15] and as biosensors [16,17].

Interestingly, since the late nineties porphyrins and metalloporphyrins have shown a new intriguing application as catalysts for organic dyes [18-20]. The later species are omnipresent in many industries like paper, food, textile, and leather. Organic dyes constitute therefore a large part of water pollutants which cause severe problems for the ecosystem and mankind. Note that vat yellow 1 dye, with the *IUPAC* name benzo[h]benz[5,6]acridino[2,1,9,8-klmna]acridine-8,16-dione (Scheme 1), belongs to the anthraquinone-type compounds presenting an intense absorption band at ~425 nm. These dyes which are extensively used for dyeing cellulosic cottons and other fibers, cause environmental concerns when released in industrial wastewaters due to their carcinogenic health effects [21]. This is why the removal of this organic species from the aqueous media is essential.

Several methods have been used for wastewater treatment including adsorption, biodegradation and photodegradation [22-24]. Notably, over the last few years, our research group has published several articles concerning the use of metalloporphyrins as catalysts for the degradation of some dyes [25-27]. Herein, we describe the synthesis of a new cobaltous meso-(arylporphyrin namely the (hexamethylenetetramine)[*meso*-tetra(*para*-methoxyphenyl) porphyrinato]cobalt(II) chloroform disolvate coordination compound with the formula $[Co^{II}(TMPP)(HMTA)]^{\bullet}\ 2CHCl_3$ (**I**) (TMPP = *meso*-tetra(*para*-methoxyphenyl)porphyrinato and HMTA = hexamethylenetetramine). The title compound was fully characterized by UV-visible titration, ^{1}H NMR, IR, mass spectrometry, cyclic voltammetry and magnetic susceptibility. The X-ray molecular structure at room temperature and at low temperature was determined. A DFT-based reactivity study of this species is also reported. The second part of this article, which is the main objective of this work, concerns the use of our hexamethylenetetramine-cobaltous porphyrin derivative (I) as a catalyst of the degradation of the vat yellow 1 dye by using a hydrogen peroxide aqueous solution and by photodegradation under solar light.

2. Experimental section

2.1. Materials and methods

All reagents employed were commercially available and were used as received without further purification. The *meso*-tetra(*para*-methoxyphenyl)porphyrin (H_2TMPP) was synthesized and purified by using the Adler-Longo method [28]. The $[Co^{II}(TMPP)]$ starting material was synthesized according to the standard literature method [29]. All reactions and manipulations for the preparation of the Co(II) porphyrin derivatives were carried out under aerobic conditions.

UV-visible, FT-IR and NMR data: The UV-visible spectra and titrations were recorded with a WinASPECT PLUS (validation for SPECORD PLUS version 4.2) scanning spectrophotometer. Fourier transform IR spectra were recorded on a PerkinElmer Spectrum Two FT-IR spectrometer. ^{1}H NMR spectroscopic characterization were performed with a Bruker DPX 400 spectrometer. Chemical shifts are reported in ppm downfield from internal tetramethylsilane (TMS).

Fluorescence data: Emission spectra were recorded in dichloromethane at room temperature on a Horiba Scientic Fluoromax-4 spectrofluorometer. Samples were placed in 1 cm path length quartz cuvettes. Luminescence lifetime measurements were performed after irradiation at $\lambda = 430$ nm obtained by the second harmonic of a titanium: Sapphire laser (picosecond Tsunami laser spectra physics 3950-M1BB + 39868-03 pulse picker doubler) at an 800 kHz rate of repetition. For the decay acquisition, Fluotime 200 (AMS technologies) was utilized consisting of a GaAsmicro channel plate photomultiplier tube (Hamamatsu model R3809U-50) followed by a time-correlated single photon counting system from Picoquant (PicoHarp300). The ultimate time resolution of the system is close to 30 ps. Luminescence decays were analyzed with FLUOFIT software available from Picoquant. Emission quantum yields were determined at room temperature in dichloromethane solutions using the optically dilute method. [Zn(TPP)] in air-equilibrated dichloromethane solution was used as quantum yield standard ($\phi_f = 0.031$)

Electrochemistry: Cyclic voltammetry (CV) experiments were performed with a CH-660B potentiostat (CH Instruments). All analytical experiments were conducted at room temperature under an argon atmosphere (argon stream) in a standard one-compartment, three-electrode electrochemical cell. Tetra-*n*-butylammonium perchlorate (TBAP) was used as the supporting electrolyte (0.2 M) in dichloromethane previously distilled over calcium hydride under argon. An automatic Ohmic drop compensation procedure was systematically implemented before the CV data were recorded with electrolytic solutions containing the studied compounds at concentrations of ca. 10^{-3} M. CH Instruments vitreous carbon ($\phi = 3$ mm) working electrodes were polished with 1 μm diamond paste before each recording. The $Ag/AgNO_3$ 0.01 M (TBAP 0.2 M in CH_2Cl_2) redox couple was used as the ence electrode. The potential of the ferrocene/ ferrocenium redox couple was used as an internal reference (86 mV vs. $Ag/AgNO_3$ under our experimental conditions). For comparison with previously published data, all potentials given in the text and in Table 7 have been converted to values relative to the saturated calomel electrode (SCE) by using the following relationship: $E(SCE) = E(Ag/AgNO_3) + 298$ mV.

Electrospray (ESI) MS: Spectra were obtained using an amaZon speed instrument. The sample made by a 5.10^{-3} M in dichloromethane was diluted to a 5.10^{-5} M solution in acetonitrile.

MALDI-TOF MS: A PerSeptive Voyager DE-STR MALDI-TOF mass spectrometer (PerSeptive Biosystems, Framingham, MA, USA), equipped with a 337 nm pulsed nitrogen laser (20 Hz) and an Acqiris 2 GHz digitizer board, was used for all experiments. Mass spectra were obtained in the positive ion mode with the following settings: accelerating voltage 20 kV, grid voltage 62% of accelerating voltage, extraction delay time of 100 ns. The laser intensity was set just above the ion generation threshold to obtain peaks with the highest possible signal-to-noise (S/N) ratio without significant peak broadening. All data were processed using the Data Explorer software package (Applied Biosystems). *Trans*-2-[3-(4-*tert*-Butylphenyl)-2-methyl-2propenylidene] malonitrile (DCTB), used as the matrix for MALDI-TOF MS, was of the highest grade available and used without further purification). It was purchased from Sigma Aldrich Co. The samples were made as 3.10^{-3} M in tetrahydrofuran (THF).

SQUID data: Temperature-dependent magnetic susceptibility measurements on polycrystalline samples of (**I**) were carried out on a Quantum Design MPMS SQUID susceptometer equipped with a 7 T magnet and operating in the range of temperature from 1.8 to 400 K. The compacted powdered samples were placed in a diamagnetic sample holder and the measurements were realized in a 1000 Oe applied field using the extraction technique. Magnetization versus magnetic field measurements of (**I**) was carried out at 2 K in the field range 0–5 T. The amount of material used for the measurements was 11.05 mg for (**I**). Before analysis, the experimental susceptibility was corrected from the sample holder's. Diamagnetic corrections of the constituent atoms of (**I**) was estimated from Pascal constants with values -295.10^{-6} -351.10^{-6} $cm^3.mol^{-1}$ respectively. [30]

Computational details: Hirshfeld surfaces and DFT approach: 3D Hirshfeld surfaces and their associated 2D fingerprint maps were drawn using the CrystalExplorer17.5 program [31] and TONTO system [32,33] The 3D d_{norm} surfaces are mapped over a fixed color scale of -0.15 a.u (red) to 1.15 a.u (blue). The shape index and curvedness mapping ranges are -1.0 to 1.0 Å and -4.0 to 0.4 Å, respectively. The Fingerprint cards were mapped by using the translated 1-3 Å, and filtering by element.

Density functional theory (DFT) calculations were performed to investigate the HOMO–LUMO energy gap of (**I**) starting from the experimental single-crystal X-ray structure as input geometries. The Gaussian 09, RevD.01 software package on a personal computer [34] was used for all calculations. The molecular surfaces properties were visualized by the GaussView 6.0 program. [35] The geometry optimization presented here was accomplished in the gas phase as a spin unrestricted open-shell system, using Becke's three parameter hybrid exchange and the nonlocal correlation functional of Lee, Yang and Parr (UB3LYP) [36-38]. A quasi-relativistic Stuttgart/Dresden (SDD) effective core potential was used on Co, [39] and 6-31G(d) was used for all other elements. Frequency calculations on optimized geometry ensured that structures were minima (zero imaginary frequency) on the potential energy surface. On the basis of this optimized molecular geometry, more accurate energies were obtained by performing SP single-point calculations with a larger standard basis set 6-311+G(d,p)/SDD. This level of theory has been found to be a robust choice for the study of cobalt(II) complexes [40,41].

Adsorption, oxidation and photodegradation of the vat yellow 1 dye: The experiments were carried out at room temperature using 5 mg of H_2TMPP and [Co^{II}(TMPP)(HMTA)] **(I)** and 5 mL of an aqueous solution of the vat yellow 1 dye at pH = 6. The stirring was kept at 200 rpm for 2 hours. The resultant mixture was filtrated and then the concentration was determined by measuring the absorption at 422 nm.

2.2. Synthesis of [Co^{II}(TMPP)(HMTA)]•2$CHCl_3$ *(I)*

The [Co^{II}(TMPP)] starting material (50 mg, 0.06 mmol) and 1,3,5,7-tetraazatricyclo[3.3.1.13,7]decane known as hexamethylenetetramine (HMTA) (80 mg, 0.6 mmol.) were dissolved in chloroform (10 mL). The obtained reaction mixture was stirred for 4 hours then overlayed by n-hexane. Dark purple crystals, suitable for X-ray diffraction, were obtained within one week and the yield was about 80 %. Elemental analysis (%) calcd for $C_{56}H_{50}Cl_6CoN_8O_4$ (1170.71): C, 57.45; H, 4.30; N, 9.57; found: C, 57,87; H, 4.21; N, 9.88; UV-visible: λ_{max} (nm, CH_2Cl_2, $\varepsilon.10^{-3}$ $L.mmol^{-1}.cm^{-1}$): 426 (276), 533 (17) nm. FT-IR (solid, cm^{-1}): 2925 [ν(CH) porphyrin], 2953, 2835 [ν(CH) methoxy], 1000-1200 [ν(CO) methoxy], 994 [δ(CCH) porphyrin], 1240 [ν(CN) HMTA]; MS MALDI-TOF (+, {(2E)-2-Methyl-3-[4-(2-methyl-2-propanyl)phenyl]-2-propen-1-ylidene}malononitrile known as trans-2-[3-(4-tert-Butylphenyl)-2-methyl-2-propenylidene]malononitrile matrix (DCTB), THF): m/z = 791.77 [Co^{II}(TMPP)]$^+$ found m/z = 791.22; MS (ESI+, CH_2Cl_2): *m/z* = 791.77 [Co^{II}(TMPP)+H]$^+$ found 792.30; m/z = 933.96 [Co^{II}(TMPP)(HMTA)+H]$^+$ found 932.30 (Figure S1); ^{1}H NMR (400 MHz, $CDCl_3$): δ = 12.68 (s, 8 H), 9.00 (s, 8 H), 8.02 (s, 8 H), 4.42 (s, 12 H), 1.58 (s, 12 H) (Figure S2).

2.3. X-ray structure determination

A single crystal with dimensions of 0.34 mm x 0.27 mm x 0.22 mm suitable for single crystal X-ray diffraction was selected and mounted on a glass fiber on an D8 VENTURE Bruker AXS equipped with graphite monochromated Mo Kα radiation (λ = 0.71073 Å) and intensity data were collected by the narrow frame method at 150(2) K (low temperature LT) and 295(2) K (room temperature RT). Data were corrected for absorption effects by the Multi-Scan method [42]. The structures were solved by the direct methods using SIR-2004 [43] and refined by full-matrix least-squares on F^2 using the SHELXL-2014 program [44]. The crystallographic data, the structural refinement details, and selected bond lengths and angles for (**I**) at low-temperature and at room temperature are reported in Table 1 and Tables S1-a-b respectively.

3. Results and discussion

3.1. ^{1}H NMR and IR spectroscopy

Cobalt(III) and cobalt(II) metalloporphyrins are diamagnetic and paramagnetic species, respectively, with 3d [6] and 3d [7] ground state electronic configurations of the Co(III) and the Co(II) cations, respectively. Therefore, ^{1}H NMR is a very convenient technique to differentiate between diamagnetic cobaltic and paramagnetic cobaltous coordination compounds. [45] Indeed, for cobalt(III) *meso*-phenylporphyrins, the signals of the β-pyrrolic and the phenyl ring protons are slightly shifted compared to those of the corresponding free base porphyrins with a chemical shift values in the order of 8.6 and 9 ppm for the β-pyrrolic protons and between 8.5 and 7.5 ppm for the phenyl protons (Table 2). In the case of Co(II) complexes with *meso*-phenylporphyrins, the β-pyrrolic and the phenyl protons ($H_{o,o'}$, $H_{m,m'}$ and H_p) peaks are downfield shifted with δ values between 12 and 16.5 ppm for the former protons and 13 to 8.5 for the later porphyrinic protons (Table 2). It is noteworthy that for [Co^{II}(Porph)] complexes, where Porph is a *meso*-aryporphyrin, the chemical shift (δ) values of the porphyrin protons are quite higher than those of the cobalt(II) pentacoordinated metalloporphyrins (Table 2). The reason is not very clear, but it has been noticed by Shirazi *et al.* [6] that for five-coordinated Co(II) *meso*-porphyrin species, e.g. [Co^{II}(TPP)(py)], the δ values of the porphyrin's protons are close to those of the diamagnetic Co(III) porphyrins and that the signals become more broad and specially the one of the β-pyrrole protons is very broad. For our synthetic compounds H_2TMPP, [Co^{II}(TMPP)] and [Co^{II}(TMPP)(HMTA)] (**I**), the chemical shift values of the β-pyrrole and the phenyl protons are reported in Table 2 and the spectra are illustrated by Figures S3, S4 and S5 respectively indicating clearly that complex (**I**), in $CDCl_3$ solution, is a cobalt(II) paramagnetic metalloporphyrin. We also noticed that the chemical shift values of the OCH_3 protons at the *para*-phenyl positions of the TMPP moiety are 4.10, 5.25 and 4.42 ppm for the H_2TMPP, [Co^{II}(TMPP)] and [Co^{II}(TMPP)(HMTA)] species, respectively, which is in accordance with what mentioned above.

On the other hand, the ^{1}H NMR spectrum of (**I**) confirms the coordination of the HMTA axial ligand where the twelve CH_2 proton of this ligand resonate at 1.58 ppm. These protons are upfield shifted compared to those of the free HMTA species (δ = 4.55 ppm) and to those of the related magnesium [Mg^{II}(TPBP)$(HMTA)_2$] (TPBP = (*meso*-tetrakis[4(benzoyloxy)phenyl]porphinato) zinc(II)

Table 1
Crystal data and structural refinement for $[Co^{II}(TMPP)(HMTA)]^{\bullet}2CHCl_3$ (**I**).

Low temperature structure	Room temperature structure	
Formula	$C_{56}H_{50}CoN_8O_4$	$C_{56}H_{50}CoN_8O_4$
Crystal System	monoclinic	monoclinic
Crystal	$P2_1/n$	$P2_1/n$
a (Å)	14.0955(15)	14.1478(13)
b (Å)	17.131(2)	17.1087(19)
c (Å)	22.298(3)	22.6816(25)
β (°)	95.159(4)	94.648(4)
V(Å^3)	5362.4(11)	5472.0(10)
Z	4	4
$\rho_{calc.}$/ g cm^{-3}	1.450	1.421
μ/ mm^{-1}	0.674	0.661
F(000)	2412	2412
Crystal size (mm^3)	0.34 × 0.27 × 0.22	0.34 × 0.27 × 0.22
Crystal Color	blue	blue
Crystal Shape	prism	prism
T(K)	150 (2)	295 (2)
θ_{min} - θ_{max} (°)	2.144 – 25.000	2.127-24.999
Limiting indices	-16 ≤ h ≤ 16, -20 ≤ k ≤ 17, -26 ≤ l ≤ 26	-16 ≤ h ≤ 16, -20 ≤ k ≤ 18, -26 ≤ l ≤ 26
R(int)	0.0401	0.0505
Reflections collected/unique	30996 / 9342	35411/9455
Observed data [$I_o > 2\sigma(F_o)$]	7739	6844
Parameters/Rest	676 / 0	677 / 6
S [Goodness of fit]	1.045	1.027
R_1[a], wR_2[c] [$F_o > 4\sigma(F_o)$]	R_1 = 0.0519, wR_2 = 0.1329	R_1 = 0.0862, wR_2 = 0.2358
wR_2[b] *[all data]*	R_1 = 0.0649, wR_2 = 0.1426	R_1 = 0.1162, wR_2 = 0.2634
Min./max. res. (eÅ^{-3})	0.993 / -1.065	1.186/-0.918
CCDC	1908123	1908124

[a] $R1 = \Sigma||Fo| - |Fc||/\Sigma|Fo|$
[b] $wR2 = \{\Sigma[w(|Fo|^2 - |Fc|^2)^2]/\Sigma[w(|Fo|^2)^2]\}^{1/2}$.

Table 2
Chemical shift values for selected free base *meso*-arylporphyrins and cobalt *meso*-arylporphyrin complexes from ^{1}H NMR spectra recorded in $CDCl_3$.

Compound	Hβ-pyrrolic protons	H-phenyl protons	H-OCH_3[a]	Ref.
Meso-porphyrins				
H_2TPP[b]	8.84	8.23; 7.91; 7.67; 7.26	-	**48**
H_2TpivPP[c]	8.82	8.70; 7.88; 7.50	-	**48**
H_2TMPP	8.86	8.08; 7.27;	4.10	this work
Co(III)-meso-porphyrins				
$[Co^{III}(TPP)Cl(py)]$[b]	9.00	8.80; 7.70	-	**49**
$[Co^{III}(TPP)(N_3)(py)]$[b]	9.22	8.38; 7.80	-	**49**
$[Co^{III}(TPP)Cl(DMI)]$[b,d]	8.83	7.87; 7.65	-	**50**
$[Co^{III}(TPP)(DMI)]^+$[b,d]	8.95	7.86; 7,71	-	**50**
Co(II)-meso-porphyrins				
$[Co^{II}(TMPP)]$	15.90	13.10; 9.43	5.25	this work
$[Co^{II}(TPP)]$[b]	15.75	13.10; 9.80; 7.95	-	**48**
$[Co^{II}(TpivPP)]$[c]	15.30	11.50; 10.90; 7.80	-	**48**
$[Co^{II}(TPP)(py)]$[b]	12.50	8.5; 8.33; 7.82	-	**6**
[Co(TPP)(HIm)][b,e]	12.8	8.8; 8,40; 7.69	-	**6**
$[Co^{II}(TMPP)(HMTA)]$	12.68	9.00; 8.02	4.42	this work

[a]: H-OCH_3= protons of the OCH_3 group in the *para*-phenyl positions of the H_2TMPP porphyrin
[b]: TPP = *meso*-tetraphenylporphyrinato
[c]: TpivPP = *meso*-[$\alpha,\alpha,\alpha,\alpha$-tetrakis(*o*-pivalamidophenyl)]porphyrinato
[d]: DMI = N,N'-dimethylimidazolylidene
[e]: HIm = imidazole.

$[\{Zn(TPP)\}_2(HMTA)]$ (TPP = *meso*-tetraphenylporphyrinato) complexes with values of 3.03 and 2.74 ppm, respectively [46,47].

The IR spectrum of $[Co^{II}(TMPP)(HMTA)]$ (**I**) is characteristic of a metalloporphyrin complex with the two typical absorption bands of the metallated porphyrin ν(CH) and δ(CHC) vibrations which appear in the [3000-2850] cm^{-1} region and at ca 1000 cm^{-1}, respectively. The majority of the absorption bands of the HMTA axial ligand are superposed with those of the TMPP porphyrinate but the HMTA presents also a weak absorption band, attributed to the N-C stretching, at 847 cm^{-1} and two deformation vibration bands [δ(NCN)] (with medium intensities) at 691 and 664 cm^{-1} [46].

3.2. UV-visible titration

As mentioned above, cobaltous metalloporphyrins can exist, in non-aqueous solutions, as four-coordinated complexes type $[Co^{II}(Porph)]$, pentacoordinated species type $[Co^{II}(Porph)(L)]$ (L is a neutral axial ligand) and rarely as hexacoordinated derivative type $[Co^{II}(Porp)(L)_2]$. It is worth noting that the UV-visible titrations of the starting material $[Co^{II}(Porph)]$ with numerous N-donor ligands such as pyridine and imidazole and their derivatives have been reported in the literature since the early seventies especially by Walker *et al.* [5] and Yamamoto *et al.* [51]. The titrations show that in major cases the 1:1 Co(II) porphyrin-L (L = N-bonded neutral ligand) species are forms [Eq. (a)] rather than the 1:2 Co(II)

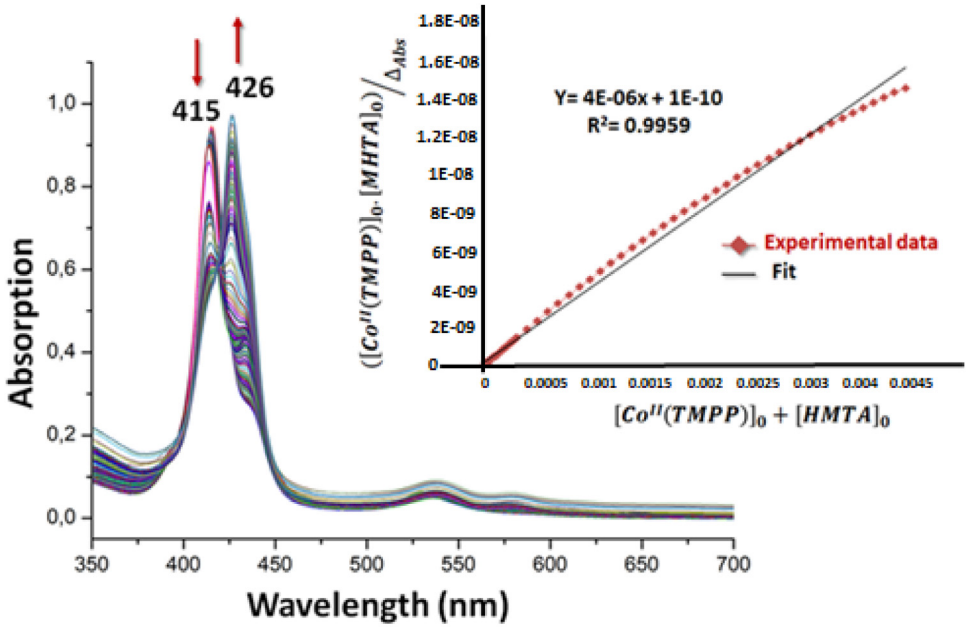

Fig. 1. Changes in the absorption spectra in the Soret band region of [Co^{II}(TMPP)] (~10^{-6} M) recorded in dichloromethane, upon addition of HMTA. Inset: the Benesi-Hildebrand plot at 415 nm with a 1:1 fit (0 - 8000 equiv.).

porphyrin-2L coordination compounds [Eq. (b)]. K_1 (known also as K_{as}) and K_2 are the association constants corresponding to equilibrium (a) and (b) respectively.

$$[Co^{II}(Porph)] + L \underset{}{\overset{K_1}{\rightleftharpoons}} [Co^{II}(Porph)L] \quad ; \qquad (a)$$

$$[Co^{II}(Porph)] + 2\,L \underset{}{\overset{K_2}{\rightleftharpoons}} [Co^{II}(Porph)(L)_2] \quad ; \qquad (b)$$

Dolphin *et al.* [52]. reported that Co(II) readily forms five-coordinate complexes but the formation of the six-cooordinate system is disfavored due to the destabilization of the d_{z^2} orbital. For the *meso*-[tetraphenylporphyrinato]cobalt(II) [Co^{II}(TPP)] and the *meso*-tetrakis[(*p*-methoxyphenyl)porphyrinato] cobalt(II) [Co^{II}(TMPP)], only the first association constants (K_1) for ligand binding could be determined. In the case of the later species, this is due to the presence of the methoxy groups in the *para* position of the phenyls of the TMPP porphyrinate which are good σ-donors leady to the increase of the electron density on the Co(II) metal ion. This makes it more difficult to a second axial ligand to be coordinated to the central metal. However, values for the second axial association constants (K_2) are known for Co(II) complexes of electron deficient porphyrins such as 2,3,12,13-tetracyano-[*meso*-tetraphenylporphyrinato]cobalt(II) [Co(TPP(CN)$_4$], [53] 2,3,7,8,12,13,17,18-octafluoro-[*meso*-tetraphenylporphyrinato]cobalt(II) [Co(TPPF$_8$)] and 2,3,8,12,13,17,18-octafluoro-[*meso*-tetrakis(pentafluorophenyl)porphyrinato]cobalt(II) [Co^{II}(TPFPPF$_8$)] [54]. On the other hand, we reported the synthesis, the spectroscopic and the X-ray molecular structures of the two hexacoordinated cobalt(II) metalloporhyrins: [Co^{II}(TPP)(Hon)$_2$] (Hon = 2-aminophenol) [11] and the [Co^{II}(TpivPP)(4,4'-bpy)$_2$] (TpivPP = $\alpha,\alpha,\alpha,\alpha$-(tetrakis(*o*-pivalamidophenyl)porphyrinato) [48]. In fact, this later species is a polymer in solid state. This means that some Co(II) hexacoordinated can be formed even with electron deficient porphyrintes such as TPP and TpivPP. Inspection of Fig. 1 shows that tetracoordinated Co(II) metalloporphyrins exhibit a Soret band value at ~ 412 nm and a Q band value at ~ 528 nm including our starting material [Co^{II}(TMPP)]. A dichloromethane solution of our complex [Co^{II}(TMPP)(HMTA)] (I) presents a Soret and Q bands band values of 426 nm 533 nm respectively. For the related Co(II) five-coordinate species [Co^{II}(TMPP)(pip)] [55] and [Co^{II}(TMPP)(py)] [5] (Table 3), the Soret band values of these two coordination compounds are not reported but the values of λ_{max} of the Q bands are 532 and 535 nm, respectively, which are very close to that of complex (I). These results clearly indicate that in solution, complex (I) is a penta-coordinated species. For haxacoordinated Co(II) *meso*-porphyrin complexes we noticed that the spectra are redshifted compared to those of the pentacoordinated cobaltous metalloporphyrins (Table 3). In the case of Co(II)-*meso*-porphyrins with the pyridine axial ligand, for the TPP porphyrinato, the logK_{as} (or logK_1) value is 2.90 while for the TMPP porphyrinate (with a OMe groups in the *para*-phenyl positions), the logK_{as} value is smaller (2.83) (Table 4). The value of logK_{as} for the [Co^{II}(T(o-OCH$_3$)PP)(py)] complex is smaller (2.68) with the T(o-OMe)PP porphyrinato bearing ortho OMe groups of the phenyls [56]. For the same pyridine axial ligand, the [Co^{II}(TPFPPF$_8$)(py)] complex with the electron deficient TPFPPF$_8$ porphyrinate, the logK_{as} value is quit high (5.6). [54] From the same Table 4 we also noticed that for the same TPP porphyrinate, the logK_{as} values depend on the axial ligands. Thus, for the [Co^{II}(TPP)(pip)] (pip = pipyridine), [51] [Co^{II}(TPP)(1-MeIm)] (1-MeIm = 1-methylimidazole) [51], [Co^{II}(TPP)(py)] [56] and [Co^{II}(TPP)(4-CNpy)] complexes, [56] the logK_{as} values are 3.51, 3.38, 2.90 and 2.76, respectively. Accordingly, if we neglect the solvent effect, the pip and the 1-MeIm ligands are much more easy to coordinate to [Co^{II}(TPP)] than the 4-CNpy ligand.

In order to calculate the association constant K_{as} of complex (I), a UV-visible titration of the [Co^{II}(TMPP)] starting material was carried out in dichloromethane with concentrations of about 10^{-6} M. Upon the addition of incremental amounts of HMTA to [Co^{II}(MPPP)], a redshift of the Soret band is observed from 414 to 426 nm with one distinct isosbestic point at 419 nm indicating clearly the formation of a 1:1 [Co^{II}(TMPP)]-HMTA species (Fig. 1). For our HMTA-Co(II) complex with the electron rich TMPP porphyrinato, the logK_{as} value is 4.33 (Table S2) which is quite higher than those of the [Co(TMPP)(pip)] [55] and [Co^{II}(TMPP)(1-

Table 3
UV-visible. data of complex (I) and a selection of Co(II) *meso*-arylporphyrin coordination compounds.

Complex	Soret band λ (nm)	Q bands λ (nm)	Solvent	Ref.
Cobalt(II) tetracoordinated complexes type [Co^{II}(Porph)]				
[Co^{II}(TPP)]	412	528	CH_2Cl_2	**48**
[Co^{II}(TpivPP)]	412	426	chlorobenzene	**48**
[Co^{II}(TMPP)]	414	429	CH_2Cl_2	this work
Cobalt(II) pentacoordinated complexes type [Co^{II}(Porph)L]$^{\pm m}$				
[Co^{II}(TMPP)(HMTA)]	426	533	CH_2Cl_2	this work
[Co^{II}(TMPP)(pip)]	-	532	CH_2Cl_2	**55**
[Co^{II}(TMPP)(py)]	-	535	toluene	**5**
Cobalt(II) hexacoordinated complexes type [Co^{II}(Porph)$(L)_2$]				
[Co^{II}(TPP)$(amp)_2$]	434	555	CH_2Cl_2	**11**
[Co^{II}(TpivPP)$(4,4'\text{-bpy})_2$]n	436	545	chlorobenzene	**48**

Table 4
Association constant [a] values of several five-coordinated cobalt(II) metalloporphyrins.

Complex	logK_{as}	Solvent	Ref.
[Co^{II}(TPP)(1-MeIm)] [b,c]	3.38	Toluene	**51**
[Co^{II}(TMPP)(1-MeIm)] [c]	3.26	Toluene	**55**
[Co^{II}(TpivPP)(2-MeIm)] [d, c]	K_{as} = 3.5 10^4 M^{-1} logK_{as} = 4.54	Benzene	**56**
[Co^{II}(T(o-OCH_3)PP)(1-MeIm)] [e,c]	3.37	CH_2Cl_2	**5**
[Co^{II}(TPP)(1,2-Meim)] [b,f]	2.91	Toluene	**56**
[Co^{II}(TPP)(py)] [b]	2.90	Toluene	**56**
[Co^{II}(TMPP)(py)]	2.83	Toluene	**56**
[Co^{II}(T(o-OCH_3)PP)(py] [e]	2.68	CH_2Cl_2	**56**
[Co^{II}(TPFPPF$_8$)(py)] [g]	5.6	CH_2Cl_2	**54**
[Co^{II}(TPP)(4-CNpy)] [b,i]	2.76	Toluene	**51**
[Co^{II}(TPP)(pip)] [b,j]	3.51	Toluene	**51**
[Co^{II}(TMPP)(pip)] [j]	3.44	Toluene	**55**
[Co^{II}(TMPP)(HMTA)]	4.60 (weak) 3.52 (strong) 4.33 (mean)	CH_2Cl_2	this work

[a] : The values of logK_{as} were taken at room temperature
[b] : TPP = *meso*-tetraphenylporphyrinato
[c] : 1-MeIm = 1-methylimidazole
[d] : TpivPP = *meso*-(α,α,α,α-tetrakis(*o*-pivalamidophenyl)porphyrinato
[e] : T(o-OCH_3)PP = *meso*-tetrakis(p-methoxyphenyl) porphyrinato
[f] : 1,2-Meim = 1,2-dimethylimisazole
[g] : TPFPPF$_8$ = 2,3,8,12,13,17,18-octafluoro-[*meso*-tetrakis(pentafluorophenyl)porphyrinato
[i] : 4-CNpy = 4-cyanopyridine
[j] : pip = piperidine.

MeIm)] [55] related species, with logK_{as} values of 3.44 and 3.26, respectively. Therefore, we can conclude that the HMTA species is a quite strong ligand in the non-coordinated dichloromethane solvent. This is confirmed by the presence in solution of the $[Co^{II}(TPP)(HMTA)+H]^+$ fragment in the ESI mass spectrometry spectrum and by ^1H NMR data.

These results indicate that the association constant value for *meso*-arylporphyrins didn't depend too much on the nature of the donor-withdrawing groups in the phenyl groups of the *meso*-arylporphyrin but depend essentially on the type of the axial ligand. This is not the case when the β-pyrrolic positions of the porphyrin are occupied by strong withdrawing halogen groups which exhibit very important distortion of the porphyrin core of these metalloporphyrins leading to an important redshift of the absorption bands [57].

3.3. Fluorescence spectroscopy

The fluorescence emission spectrum of our Co(II)-HTMA-TMPP derivative (I) recorded at room temperature in dichloromethane upon photoexcitation at the wavelength 430 nm exhibits two emission bands $S_1 \rightarrow S_o$ allocated as the Q(0,0) and Q(0,1) transitions (Fig. 2). The λ_{max} values of the Q(0,0) and Q(0,1) emission bands of **(I)** are 652 nm and 718 nm, respectively which are very close to the related Co(II) meso-arylporphyrin species such as $[Co^{II}(TMPP)(4\text{-CNpy})]$ (4-CNpy = 4-cyanopyridine) [27]. For this later species the λ_{max} values of the Q(0,0) and Q(0,1) bands are 652 nm and 717 nm, respectively.

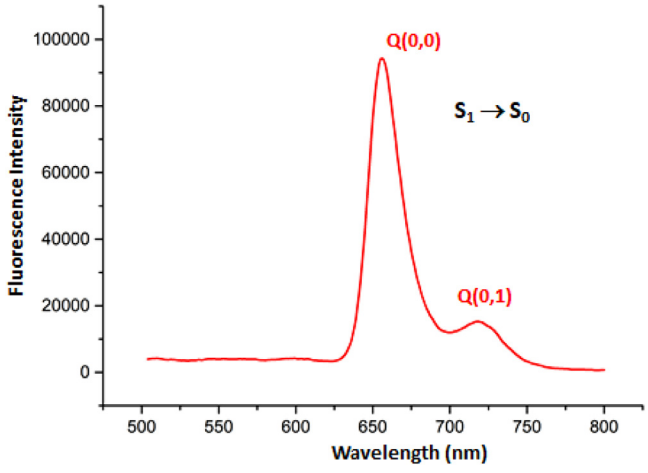

Fig. 2. Emission spectra of **(I)** recorded at room temperature in dichloromethane (concentrations ~ 10^{-6} M).

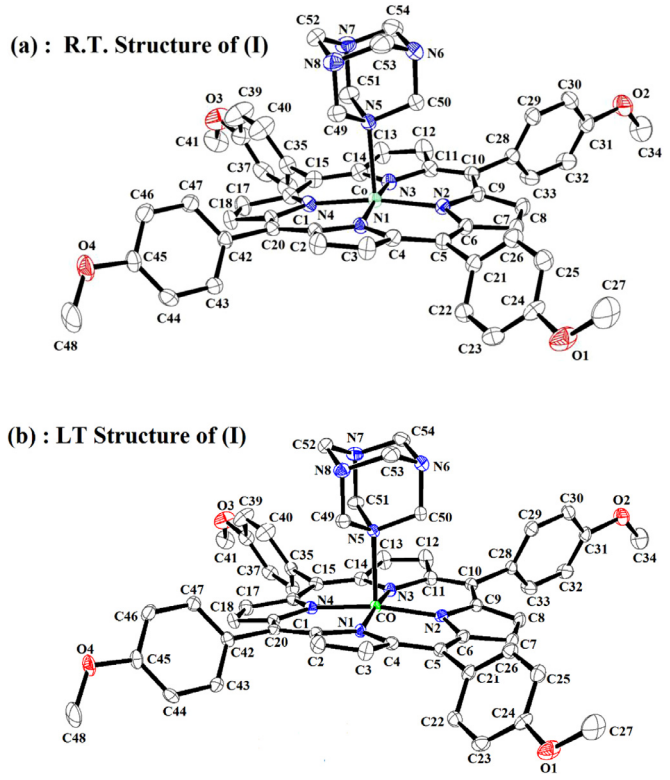

Fig. 3. Ortep diagrams of [Co^{II}(TMPP)(HMTA)]. Ellipsoids are contoured at the 30% probability for the structure at RT **(a)** and 50% probability of the structure at LT **(b)**.

The fluorescence quantum yields Φ_f and the lifetime of singlet excited state τ_f values of (**I**) and the

[Co^{II}(TMPP)(4-CNpy)] [27] related species are very close. Thus, the (Φ_f) and the τ_f) values are 0.028 and 1.53 nm, respectively for our Co(II)-HMTA derivative (**I**) and 0.054 and 1.97 nm for the related Co(II)-4-CNpy species. Notably, the fact that the [Co^{II}(Porph)(L)] (Porph = *meso*-arylporphyrin and L is a N-donor neutral axial ligand) complexes exhenit Φ_f and τ_f values smaller than the corresponding free base porphyrins is related to the paramagnetic nature of the cobalt(II) metal center which allows intersystem crossing to the triple state and hence lowering fluorescence [27-58].

3.3. X-ray structures of (I)

The single crystal molecular structure of (**I**) was determined using the same crystal at room temperature (295 K) then at low temperature (150 K) in order to check if there is any change of the structure of our Co(II)-HMTA derivative from low to room temperature. The room temperature (RT) and the low-temperature (LT) structures of (**I**) are practically the same. Indeed, this species crystallizes in the monoclinic system ($P2_1/n$ space group). The cell parameters of (**I**) at RT and LT are very close (Table 1) where the RT parameters are slightly higher (about 2%), as expected, than those of the LT with a volumes values of 5472.0(10) at 295 K and 5362.4(11) at 150 K. The asymmetric unit of (**I**) is made from [Co^{II}(TMPP)(HMTA)] complex and two chloroform molecules and both RT and LT structures of [Co^{II}(TMPP)(HMTA)].2$CHCl_3$ (**I**) are illustrated in Fig. 3. The Co^{2+} cation is chelated by the four pyrrole N atoms of the porphyrinate anion and additionally coordinated by the HMTA ligand in an apical site, completing the distorted square-pyramidal coordination environment (Figure S6).

It is noteworthy that hexamethylenetetramine metalloporphyrins are very rare and in the Cambridge data base (CSD version 5.40) only five X-ray molecular structures are reported; four with zinc(II) and one with magnesium(II) cations (Table 5). Our synthetic complex (**I**) is the first example of a Co(II) metalloporphyrin with the HMTA axial ligand. The Co—N(HMTA) bond lengths are 2.287(2)/2.296(4) Å (RT/LT) which are normal for a cobalt(II) bonded to an sp [3] hybridized nitrogen of a N-bonded axial ligand. Indeed, these values are in the [2.278 – 2.354] Å range of several HMTA-cobalt(II) non-porphyrinic species (Table 5). On the other hand, we noticed that the Co—N(HMTA) distance of our derivative is: (i) quite shorter than that of the related [Co^{II}(TPP)(pip)$_2$] [59] complex where pip is the non-aromatic piperidine ligand with a Co—N(pip) distance of 2.436 Å and (ii) this values of (**I**) are, as expected, higher than those of Co(II) metalloporphyrins with aromatic N-bonded axial ligands such as 2,6-lutidine [60] and 1-methylimidazole [61] with Co—N(axial ligand) distance values of 2.017(2) Å and 2.157(3) Å respectively (Figure S6).

Notably, the value of the mean equatorial distance between the cobalt cation and the four nitrogen atoms of the porphyrin core (Co—Np) is directly related to the *ruffling* deformation of the porphyrin macrocycle as mentioned by Iimura *et al.* [62]. Thus, the Co—Np bond length decreases as le *ruffling* of the porphyrin core increases, known that the *ruffling* distortion is indicated by the high values of the displacement of the *meso*-carbon atoms above and below the porphyrin mean plane (Figure S7). In the case of the two tetracoordinated cobalt(II) [Co^{II}(TPP)] complexes reported in Table 5, the Co—Np distances are 1.923 Å for the structure reported by Konarev *et al.* [63] and 1.949 Å for the structure reported by Nascimento *et al.* [64]. These values which are the smallest among all cobalt(II) metalloporphyrins reported in Table 5, exhibit the most *ruffled* porphyrin cores. For pentacoordinated and hexacoordinated cobalt(II) porphyrins were observe the same trend: decreasing of the Co—Np distance with increasing of the *ruffling* deformation of the porphyrin core. This is the case of the very *ruffled* structures of [Co^{II}(TPP)(NO_2)(lut)] [60] (lut = 3,5-lutidine) and [Co^{II}(TCPP)(py)$_2$] (with TCPP = *meso*-tetrakis(4-carboxyphenyl)-porphyrinato**)** [65] with a Co—Np distances of 1.959 and 1.961 Å respectively while for the planar or moderately *ruffled* Co(II) porphyrins such as [Co^{II}(TPP)(1-MeIm)] [61] and [Co^{II}(TPP)(pip)$_2$] (pip = piperidine) [59] the Co—Np distance values are longer with values of 1.978(3) and 1.987 Å respectively. For our HMTA derivative [Co^{II}(TMPP)(HMTA)] (**I**), the Co—Np bond length values are 1.975 (4) Å (RT) and 1.982(3) (LT) where the RT Co—Np distance is very close to that of the Co(II-TPP-1-MeIm) species [59] with a Co—Np value at RT of 1.978(3) Å [59]. Both complexes exhibiting, moderate *ruffling,* confirm what we just explained about the relationship between the *ruffling* deformation and the Co—Np distance. It should also be noted that the porphyrin core of our Co(II)-HMTA complex manifests also at RT and LT a moderate *saddle* deformation which is due to the displacement of the pyrrole rings alternately above and below the mean porphyrin macrocycle so that the pyrrole nitrogen atoms are out of the mean plane (Figure S7) [66]. Nevertheless, it appears that the *saddle* deformation did not affects the length of the Co—Np distance. From Fig. 4, we first notice that the values of the displacements of the porphyrin core atoms of (**I**) from the mean plane of the 24-atom porphyrin macrocycle are slightly higher for the RT structure than those of the LT structure. We also noticed that the Co^{2+} cation of (**I**) is displaced by 0.150 (1) Å (RT) and 0.141 (1) Å from the 24-atom porphyrin mean plane (P_C) which are very close to that of the [Co^{II}(TPP)(1-MeIm)] (Co—P_C = 0.139 Å) confirming the high similarity between this two coordination compounds. Furthermore, the Co—P_C distances values of (**I**) is much smaller than those of the two reported five-coordinated zinc(II)-HMTA metalloporphyrins [{Zn^{II}(TPP)}$_2$(HMTA)] and [Zn^{II}(TPyP)(HMTA)] with values of 0.337 and 0.404 Å, respectively, known that the radii of the Co^{2+} and Zn^{2+} radius are very close (0.74 and 0.72 Å, respectively).

Table 5
Selected bond lengths [Å] and angles [°] for $[Co^{II}(TMPP)(HMTA)]\cdot 2CHCl_3$ (**I**) and several hexamethylenetetramine (HMTA) porphyrinic and non-porphyrinic complexes.

Complex	Porphyrin [a]	M—N_p [b]	M—X_L [c]	M—P_C [d]	Ref.
	core deformation type				
HMTA-meso-porphyrin complexes					
$[\{Zn^{II}(TPP)\}_2(\mu_2\text{-HMTA})]$ [e]	-Ruf, Dom	2.064 (3)	2,291 (3)	0.337	[48]
$[Zn^{II}(TPyP)(HMTA)]$ [f]	-Ruf, Dom	2.105 (4)	2.191 (3)	0.405	[69]
$[Zn^{II}(TCPP)(HMTA)_2]$ [g]	Planar	2,066	2.510	0.000	[67]
$[Zn^{II}(THPP)(HMTA)_2]$ [h]	Planar	2.060	2.520	0.000	[67]
$[Mg^{II}(TPP)(HMTA)_2]$ [e]	Planar	2.067(5)	2.473 (2)	0.005	[68]
$[Mg^{II}(TPBP)(HMTA)_2]$ [h, i]	Planar	2.074	2.439	0.000	[47]
$[Co^{II}(TMPP)(HMTA)]$ (**I**)	-Ruf, Sad	1.975 (4) (RT) 1.983 (3) (LT)	2.296(4) (RT) 2.287(2) (LT)	0.150(1) (RT) 0.141(1) (LT)	this work
Co(II) meso-porphyrin complexes					
$[Co^{II}(TPP)]$ [e]	++Ruf	1.923	-	0.050	[63]
$[Co^{II}(TPP)]$ [e]	+Ruf	1.949	-	0.009	[64]
$[Co^{II}(TPP)(NO_2)(lut)]$ [e, j]	+Ruf	1.959(2) 1.925(2) (NO_2)	2.017(2)	(Lut) 0.044	[63]
$[Co^{II}(TPP)(1\text{-MeIm})]$ [e, k]	-Ruf,	1.978 (3)	2.157 (3)	0.139	[61]
$[Co^{II}(TPP)(pip)_2]$ [e,l]	Planar	1.987	2.436 (2)	0.000	[60]
$[Co^{II}(TCPP)(py)_2]$ [g]	+Ruf	1.961	1.958	0.000	[66]
HMTA -Co(II) non-porphyrinic complexes					
$[Co^{II}(OL)_2(HMTA)_2(H_2O)_2]$ [m]	-	-	2.280	-	[69]
$[Co^{II}(NCS)_2(MeOH)_2(HMTA)]$	-	-	2.278(1)		[70]
$[Co^{II}(NL)_2(H_2O)_2(HMTA)_2]$ [n]	-	-	2.360		[71]
$[Co^{II}(H_2O)_2(HMTA)_2(NCS)_2]$	-	-	2.324	-	[72]
$[\{Co^{II}(H_2O)_2(N_3)_2\}_2(\mu_2\text{-HMTA})]_n$	-	2.354	**73**		[73]

[a] : See the description of different types of the porphyrin core in the text and in Scheme S6
[b] : M—Np = average equatorial cobalt-nitrogen pyrrole distance
[c] : M—X_L = metal-axial ligand distance
[d] : M—P_C = Distance between the metal atom and the mean plane made by the 24-atom core of the porphyrin (P_C)
[e] : TPP = *meso*-tetraphenylporphyrinato
[f] TPyP = *meso*-tetrakis(4-pyridyl)porphyrinato
[g] : TCPP = 5,10,15,20-tetrakis(4-carboxyphenyl)porphyrinato
[h] : THPP = *meso*-tetrakis(4-hydroxyphenyl)porphyrinato
[i] : TPBP = *meso*-{tetrakis-[4-(benzoyloxy)phenyl]porphyrinato
[j] : Lut = 3,5-lutidine
[k] : 1-MeIm = 1-methylimidazole
[l] : pip = piperidine
[m] : OL = cinnamato-O ligand
[n] : NL = 5,5-diphenylhydantoinato.

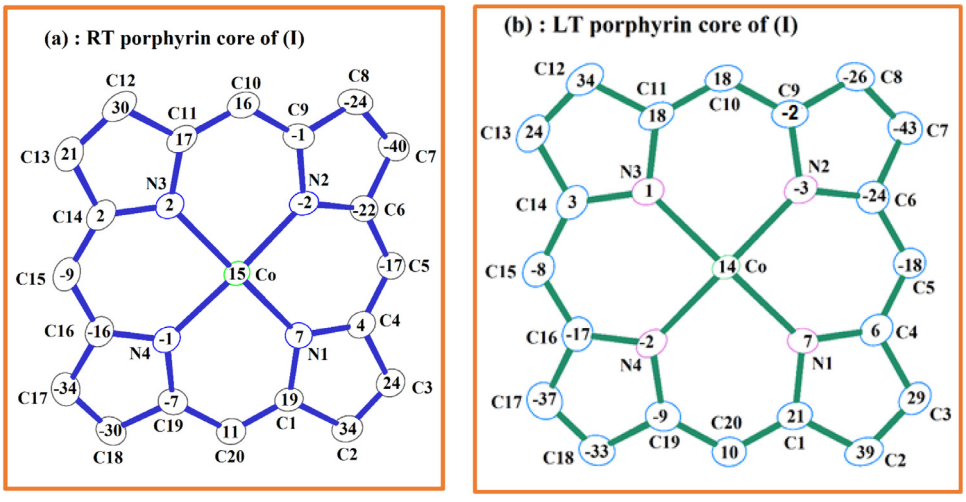

Fig. 4. Formal diagrams of the porphyrinato cores of $[Co^{II}(TMPP)(HMTA)]$ where the displacement of each atom from the mean plane of the 24-atom porphyrin macrocycle in given in units of 0.01 Å. **(a):** RT porphyrin core of (**I**), **(b):** LT porphyrin core of (**I**).

This indicates a better affinity of the HMTA ligand to the Co(II) metal ion chelated by the TMPP porphyrinato than the Zn(II) center ion complexed by the more basic PPyP porphyrinato (TPyP = *meso*-tetrakis(4-pyridyl)porphyrinato).

For the description of the crystal packing of (**I**), we are going to use the low-temperature structure data because they are better than those of the room temperature structure even though the values of the intermolecular interactions for both RT and LT structures are very close. The intramolecular and intermolecular interactions for (**I**) involves $[Co^{II}(TMPP)(HMTA)]$ molecules and chloroform solvent molecules where the cobalt(II)-HMTA porphyrin are located upside down in the lattice (Fig. 5). Indded, one $[Co^{II}(TMPP)(HMTA)]$ molecule is linked to the neighboring Co(II) complexes as follows: (i) the hydrogen H36 of the C36 carbon of a phenyl ring is hydro-

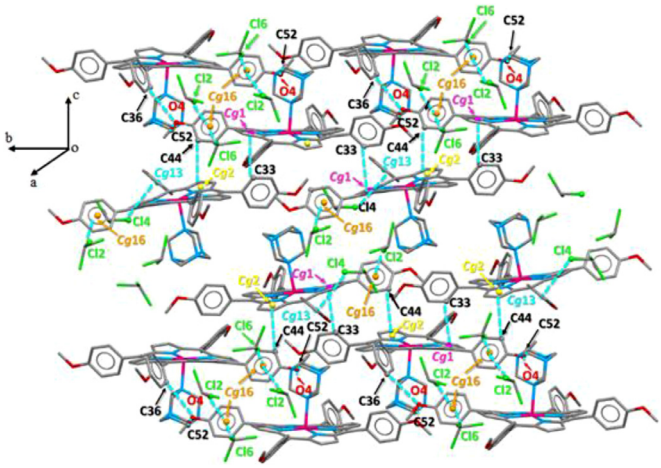

Fig. 5. Schematic representation showing the weak C—H···O, C—H···N, C—H···Cg and C—Cl···Cg intermolecular interactions of [Co^{II}(TMPP)(HMTA)].2$CHCl_3$ (**I**) where Cg is the centroid of a pyrrole or phenyl ring of the TMPP porphyrinate.

gen bonded to the oxygen atom O4 of a nearby cobaltous-complex with a C36—H36···O4 distance value of 3.591(10) Å, (ii) two hydrogen atoms of two different phenyl rings of the same TMPP porphyrinato are weakly linked each one to a centroid of a pyrrole ring of two adjacent Co-TMPP moieties with C33—H33···Cg1 and C44—H44···Cg2 distances of 3.843(4) and 3.560(4) Å (Table S3), (iii) the hydrogen H51A of the carbon C51 of one phenyl ring is also involved in a C—H···Cg intermolecular interaction with the centroid Cg3 of a nearby [Co^{II}(TMPP)(HMTA)] complex (Table S3) and (iv) one hydrogen of a methoxy group of one TMPP porphyrinato is involved in a C—H···Cg interaction with the centroid Cg14 of a phenyl ring of a nearby Co-TMPP derivative (Table S3). The HMTA axial ligand is also implicated in the crystal packing of (**I**) where the hydrogen of the carbon C52 is weakly H-bonded to the oxygen O4 of an OMe group of an adjacent TMPP-cobalt molecule. Furthermore, the chlorine atoms of the two chloroform solvent molecules play an important role on the coherence of the crystal lattice of (**I**). Indeed, the chlorines Cl2, Cl4 and Cl6 are linked to the phenyl centroids Cg13 and Cg16 via C—H···Cg intermolecular interactions (Table S3, Fig. 5) where the smallest interaction distance value is 3.560(4) Å.

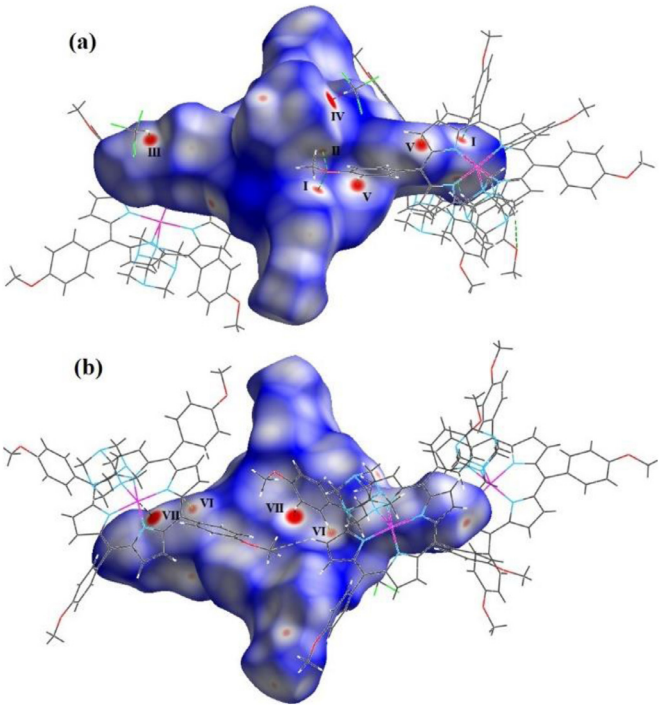

Fig. 6. Hirshfeld surface mapped with d_{norm} about a reference molecule in two different perspectives of view. Labels are discussed in the text.

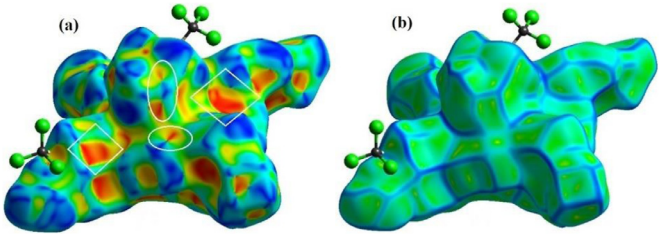

Fig. 7. Shape index **(a)** and curvedness **(b)** molecular surfaces, showing the complementary patches where π–π interactions occur. Highlighted regions are discussed in the text.

3.4. Hirshfeld surface analysis

Hirshfeld surface analysis was performed in order de better understand and highlight the contribution of significant interactions between molecules that are responsible for the molecular arrangement observed in the crystalline state. The Hirshfeld surfaces mapped with d_{norm} are illustrated in Fig. 6. The red regions labelled **I** and **II** in the d_{norm} surface are assigned to C36—H36···O4 and C52—H52A···O4 hydrogen bonds, respectively. The intense red spot (**III**), involving the acceptor O2 oxygen atoms methoxy groups of the TMPP porphyrinato is relative to strong C55—H55···O2 non classical hydrogen bond. The brightest red area labelled as **IV** is attributed to the strongest C56—H56···N8 non-conventional hydrogen bond between the carbon C55 of one chloroform molecule and the oxygen O2 of a neighboring TMPP moiety. The corresponding distance value ($d_{H\text{-}N}$ = 2.32 Å) is significantly shorter than the corresponding sum of vdW radii, indicating that these C—H···N interactions play an important role in the crystal packing. The red region (**V**) represents C···H interactions associated to C46–H46•••C18 non-classical hydrogen bonds. In addition, an unusual Co•••H contacts ($d_{H\text{-}Co}$ = 2.73 Å) are indicated as red circles (labeled **IV**) including the H32 hydrogen atom of the C28-C33 phenyl ring. The presence of π-stacking interactions is confirmed by the appearance of red and blue triangle pairs on the Shape-index surfaces identified as white circles in Fig. 7-a. Moreover, red concave regions indicate hydrogen acceptor centers, while blue convex regions designate the H donor atoms (white quadrate). The relatively large green regions, observed as flat patches in the curvedness mapped surfaces, indicate the presence of C–H···Cg π interactions between molecules (Fig. 7-b). The fingerprint (d_i versus d_e) cards of the main intermolecular interactions are shown in Figure S8. Practically all interactions occur between two chemically and crystallographically equal molecules. Thus, most maps are quite symmetric except the H···Cl/Cl···H interactions which involve the chlorine of the chloroform solvent molecules. The H•••H and C···H contacts have the most important contribution to the total Hirshfeld surface with 51.3% and 18.1%, respectively. The proportions of H···Cl and H···O contacts comprise 11.3% and 8.3% of the total map, respectively. The pair of narrow spikes pointed on a (d_e+ d_i) around 1.4 Å is attributed to the presence of O·••H interactions. The C–Cl•••Cg (π) contacts observed through experimental crystallographic study are confirmed by the presence of Cl•••C (π) which comprise 3.4% of the total. Moreover, the crystalline structure is also maintained by C···C, C···O and O···Cl contacts, even with negligible contributions.

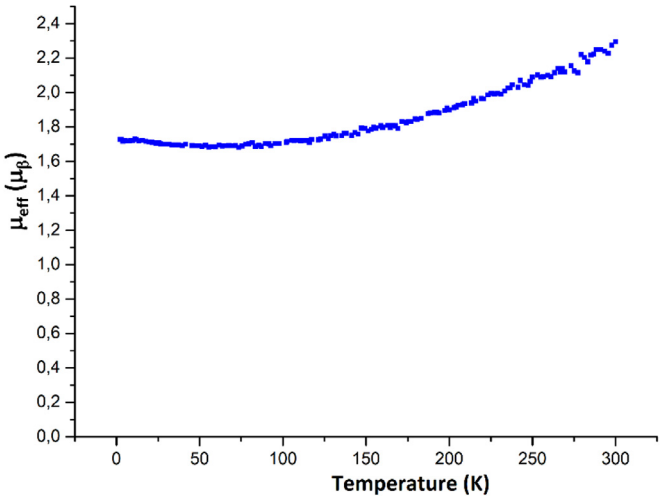

Fig. 8. Temperature dependence of the effective magnetic moment (μ_{eff}) of complex (**I**).

3.5. Magnetic properties of complex (I)

The temperature dependence of the *effective magnetic moment* (μ_{eff}) of complex (**I**) is depicted in Fig. 8 while Figure S9 illustrates the temperature dependence of $\chi_M T$ (χ_M is magnetic susceptibility) of the same species. The μ_{eff} values are 1.72 μ_β at 2.0 K and 2.28 μ_β at 300 K. While the first value is appropriate for a low-spin (LS) (S = 1/2) cobaltous derivative, the effective magnetic moment value of 2.28 μ_β at 300 K is quite bigger than that of a low-spin (S = 1/2) Co(II) species but also smaller than the theoretical spin-only μ_S value of 3.87 μ_β for a high-spin (HS) S = 3/2 cobalt(II) compound. This might result from a thermal spin-crossover between the LS state, S=1/2, $(t_{2g})^6(e_g)$ [1] and the HS state, S=3/2, $(t_{2g})^5(e_g)$ [2]. As commonly observed for SCO-active cobalt(II) complexes (SCO = spin crossover), the transition appears gradual and incomplete. Inspection of Figure S9 shows the presence of a plateau region between 2 K and 100 K, with a constant $\chi_M T$ values of ~ 0.37 emu/molOe expected for an uncoupled 1/2 ion, corresponding to the LS state (theoretical value 0.374 emu/molOe) [74].

From 100 to 300 K, the $\chi_M T$ value slowly increases as a very gradual and incomplete SCO towards the HS state occurs, to a value of 0.66 emuK/moleOe at 300 K. The field dependence of the magnetization, M = f(H), at 2 K given in Figure S10 shows that our cobaltous derivative (**I**) displays a value close to the saturation at 1 mb (0.96 μ_β with g = 2).

3.6. Cyclic voltammetry

Numerous cyclic voltammetry (CV) investigations of synthetic cobalt(II) porphyrin coordination compounds have been reported in the literature especially by Kadish *et al.* [75 76]. In the case of the *meso*-(tetraphenylporphyrinato)cobalt(II) complex [Co^{II}(TPP)], [76] it have been reported that this species in dichloromethane and nonchlorinated solvents (such as THF and DSMO) presents three one-electron reversible oxidations (Scheme 2-a) where the first one corresponds to the center metal Co(II)/Co(III) oxidation [Eq. **(I)**] followed by two ring oxidations (Eq. **(II)** and Eq. **(III)** respec-

(a) : In dichloromethane and nonchlorinated solvents:

Oxydations

$[Co^{II}(TPP)]$ ⇌	$[Co^{III}(TPP)]^+ + e^-$	Co(II)/Co(III) oxid.	**(I)**
$[Co^{III}(TPP)]^+$ ⇌	$[Co^{III}(TPP)]^{2+} + e^-$	ring oxid.	**(II)**
$[Co^{III}(TPP)]^{2+}$ ⇌	$[Co^{III}(TPP)]^{3+} + e^-$	ring oxid.	**(III)**

(b): In nonchlorinated solvents:

Reductions

$[Co^{II}(TPP)] + e^-$ ⇌	$[Co^{I}(TPP)]^-$	Co(II)/Co(I) red	**(IV)**
$[Co^{I}(TPP)]^- + e^-$ ⇌	$[Co^{I}(TPP)]^{2-}$	ring red.	**(V)**

(c) : In dichloromethane solvent:

Reductions

$[Co^{II}(TPP)] + e^-$ ⇌	$[Co^{I}(TPP)]^-$	Co(II)/Co(I) red.	**(IV)'**
$[Co^{I}(TPP)]^- + CH_2Cl_2$ →	$[Co^{I}(TPP)(CH_2Cl)] + Cl^-$		**(V)'**
$[Co^{I}(TPP)(CH_2Cl)] + e^-$ ⇌	$[Co^{I}(TPP)(CH_2Cl)]^-$	ring red.	**(VI)'**
$[Co^{I}(TPP)(CH_2Cl)]^- + Cl^-$ →	$[Co^{II}(TPP)] + CH_2Cl_2 + 2e^-$		**(VII)'**
$[Co^{II}(TPP)] + e^-$ ⇌	$[Co^{I}(TPP)]^-$	Co(II)/Co(I) red.	**(VIII)'**
$[Co^{I}(TPP)]^- + e^-$ ⇌	$[Co^{I}(TPP)]^{2-}$	ring red.	**(IX)'**

Scheme 2. Electrochemical reactions of [Co^{II}(TPP)] [75,76]. **(a):** in dichloromethane and nonchlorinated solvents, **(b):** in nonchlorinated solvents and **(c):** in dichloromethane solvent.

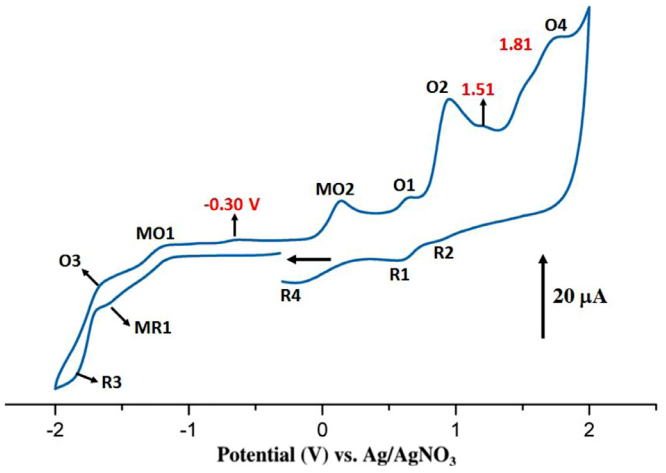

Fig. 9. Cyclic voltammogram of (**I**). The solvent is CH_2Cl_2 and the concentration is ca. 10^{-3} M in 0.2 M TBAP, **100** mV/s, vitreous carbon working electrode (Ø = 2 mm).

tively). The reduction of the same [Co^{II}(TPP)] species in nonchlorinated solvents (Scheme 2-b) [49,75,76] leads to the center metal reduction Co(II)/Co(I) [Eq. **(IV)**] followed by a second ring centered one-electron reduction at quite negative potentials [Eq. **(V)**]. The electrogenerated Co(I) porphyrin [Co^{I}(TPP)]$^-$ species is modestly stable in electrochemical nonchlorinated solvent, but rapidly reacts with CH_2Cl_2 solvent (Scheme 2-c) leading to a transient carbon-bonded species identified as the [Co^{I}(TPP)(CH_2Cl)] complex which will be reduced to the [Co^{I}(TPP)(CH_2Cl)]$^-$ species. Reactions **(VII)'** and **(VIII)'** regenerate the [Co^{I}(TPP)]$^-$ derivative and then a second irreversible ring reduction will take place [Eq. **(IX)'**]. This late electrochemical reaction is only observed in dichloromethane (Scheme 2-c) [76].

The cyclic voltammetry of our [Co^{II}(TMPP)(HMTA)] complex, shown in Fig. 9 was recorded in the non-coordinating solvent dichloromethane under an argon atmosphere using tetra-n-butylammonium perchlorate (TBAP) as the supporting electrolyte (0.2 M) and all potential values are given in volt versus SCE. The first one-electron quasi-reversible reduction corresponds to the Co(II)/Co(I) reduction [Eq. **IV'**], occurs at E_{cq} = -1.30 V (where E_{cp} is the cathodic pic) and the half potential value is $E_{1/2}$ = -1.09 V **[MR1,MO1]** (Fig. 9). As mentioned by Kadish *et al.* in the case of the [Co^{II}(TPP)], [75] the electrogenerated [Co^{I}(TMPP)(HMTA)]$^-$ is not stable and rapidly reacts with CH_2Cl_2. Consequently, reactions similar with those of equations: [Eq. **(V)'**] to [Eq. **(VIII)'**] occur leading most probably to the formation of the [Co^{I}(TMPP)(CH_2Cl)] and [Co^{I}(TMPP)(CH_2Cl)]$^-$ intermediates and may explain the presence of the irreversible wave with E_{ap} = -0.30 V (where E_{ap} is the anodic pic) [68]. A one electron quasi-reversible first ring reduction corresponding to the ring reduction (similar to Eq. **(IX)'**) is also observed with $E_{1/2}$ = -1.44 V **[R3,O3]**. The anodic part of the cyclic voltammogram of [Co^{II}(TMPP)(HMTA)] (**I**) shows that we get first a one electron irreversible oxidation of the center metal [Co(II)/Co(III) with E_{ap} = 0.25 V **[MO2]** corresponding to Eq. **(I)**, followed by a first and second oxidation of the porphyrin ring (**[O1,R1]** and **[O2/R2]** respectively) with $E_{1/2}$ values of 0.91 and 1.21 V respectively. These waves correspond to the Eq. **(II)** and Eq. (**III**). Two irreversible waves with E_{ap} values of 1.51 and 1.81 V are also shown and could be explained by the departure of the HMTA ligand leading to a unidentified reactions. Our cobaltous tetracoordinated TMPP derivative exhibits also an irreversible oxidation wave **[O4]** with E_{ap} value of 2.03 V. which can be attributed to the oxidation of the *meso*-porphyrin as reported by Simonneaux *et al.* [77]

The irreversibility of this oxidation is due to chemical reactions involving unstable electrogenerated radical leading to an unidentified species reduced at about 0.09 V **[R4]**.

As can be seen from the data of the electrochemical data reported in Table 6, we notice that (i) the half potential values of the Co(II)/Co(I) metal reduction for the tetravalent [Co^{II}(TPP)] complex and the pent-coordinated or hexa-coordinated [Co^{II}(Porp)$(L)_x$] (Porph = *meso*-porphyrin, L = N-donor axial ligand and x = 1 or 2] didn't vary too much with the solvents used, (ii) the $E_{1/2}$ of the pentacoordinated and hexacoordinated cobaltous metalloporphyrins are slightly shifted toward negative potential values compared to those of the tetracoordinated Co(II) porphyrins. On the other hand, the $E_{1/2}$ values of the Co(II)/Co(III) metal oxidation are solvent depend and that they exhibit more negative shifted $E_{1/2}$ values for pentacoordinated and hexacoordinated Co(II) metalloporphyris than the corresponding tetracoordinated cobaltous complexes. Concerning our Co(II)-HMTA derivative (**I**), the Co(II)/Co(I) $E_{1/2}$ value in CH_2Cl_2 is equal to -1.09 V which is in the range [-0.83 -1.10] V shown in several solvents for five and six-coordinated cobaltous metalloporphyrins. The half potential Co(II)/Co(III) potential value of (**I**) which is 0.25 V, is shifted to more positive potential values compared to that of the related pyridine species [Co^{II}(TPP)$(py)_x$] (x = 1 or 2), with $E_{1/2}$ = -0.12 V, where the data are recorded also in dichloromethane. The question is whether this difference is due to the nature of axial ligands (HMTA vs pyridine) or to the nature of the *meso*-porphyrin: the TPP porphyrinato vs the methoxy *para*-substited phenylporphyrinato TMPP. As mentioned above, the OMe groups in the *para*-phenyl positions of the TMPP porphyrinato increases the electron density of the Co(II) center metal and therefore complex (**I**) should be normally easy to oxidize, which is not the case, because (**I**) presents a $E_{1/2}$[Co(II)/Co(III)] value of 0.25 V. Since no electrochemical data of a HMTA-Co(II) with any other *meso*-porphyrins are available to be used for comparison, the presence of the HMTA ligand is fore probably the main reason why the Co^{2+} in (**I**) is relatively easy to oxidize. Moreover, the fact that the larger shift to more negative potential values observed for the Co(II)/Co(III) oxidation compared to those of the Co(II)/Co(I) reduction suggests that Co(III) complexes are stabilized to a greater degree than the cobalt(II) metalloporphyrin complexes. [4]

3.7. Chemical reactivity analysis

Theoretically, the chemical reactivity of a molecule can be described by using frontier orbital analysis and electronic reactivity descriptors. Herein, the electron density distribution surfaces and energies of two important molecular orbitals of the title molecule: the highest occupied molecular orbitals (HOMO) and the lowest lying unoccupied molecular orbitals (LUMO), were calculated and presented in Fig. 11. The LUMO as an electron acceptor represents the ability to obtain an electron, HOMO represents the ability to donate the electron. Hence, these orbitals determine the way the molecule interacts with other species. Moreover, the energy gap between HOMO and LUMO is a critical parameter in determining the electrical transport properties of molecules [77]. In addition, energy gap has been used to prove the bioactivity from intermolecular charge transfer [78–80]. A molecule with a small frontier orbital gap, also termed as soft molecule, is more polarizable and is generally associated with a high chemical reactivity and a low kinetic stability [81]. The difference in energy between these two frontier orbitals can be used to predict the strength and stability of transition metal complexes [82]. The size of the LUMO lobe can help predict where addition to π-ligands will occur. From Fig. 10, it is clearly seen that the HOMO and LUMO are localized on the pyrrole rings of the porphyrin parts and the N5 ligand nitrogen atom. The lowest unoccupied molecular orbital (LUMO) energy is 1.362

Table 6
Electrochemical data [a] for complex **(I)** and a selection of cobalt(II) metalloporphyrins.

	Reductions Solvent	Metal Reduction Co(II)/Co(I) (MR1,MO1) $E_{1/2}$ [b]	Ref.. Ring Reduction First red. (R3,O3) $E_{1/2}$	Metal Oxidation Co(II)/Co(III) (MO2) $E_{1/2}$	Oxidations Ring Oxidations First oxid. (O1,R1) $E_{1/2}$	Second oxid. (O2,R2) $E_{1/2}$	
[Co^{II}(TPP)]	CH_2Cl_2	-0.83	-1.40*	0.98	1.16	-	76
[Co^{II}(TPP)]	CH_2Cl_2	-	-	0.75	0.91	-	4
	PrCN[c]	-0.89	-	0.26	-	-	4
	DMF[d]	-0.84	-	-0.03	-	-	4
[Co^{II}(TPP)$(py)_x$]	CH_2Cl_2	-1.16	-	-0.12	-	-	76
	DMSO[e]	-0.99	-	-0.26	-	-	4
	DMF[d]	-0.93	-	-0.20	-	-	4
[Co^{II}(TPP)$(pip)_x$]	DMSO[e]	-0.94	-	-0.35	-	-	4
[Co^{II}(TMPP)(HMTA)]	CH_2Cl_2	-1.09	-1.44	0.25*	0.91	1.21*	this work

*: Irreversible wave
[a] The potentials are reported versus SCE
[b] $E_{1/2}$ = half wave potential
[c] : PrCN = Butanenitrile with the formula C_4H_7N
[d] : DMF = N,N-Dimethylformamide with the formula C_3H_7NO
[e] : DMSO: Dimethyl sulfoxide with the formula C_2H_6OS.

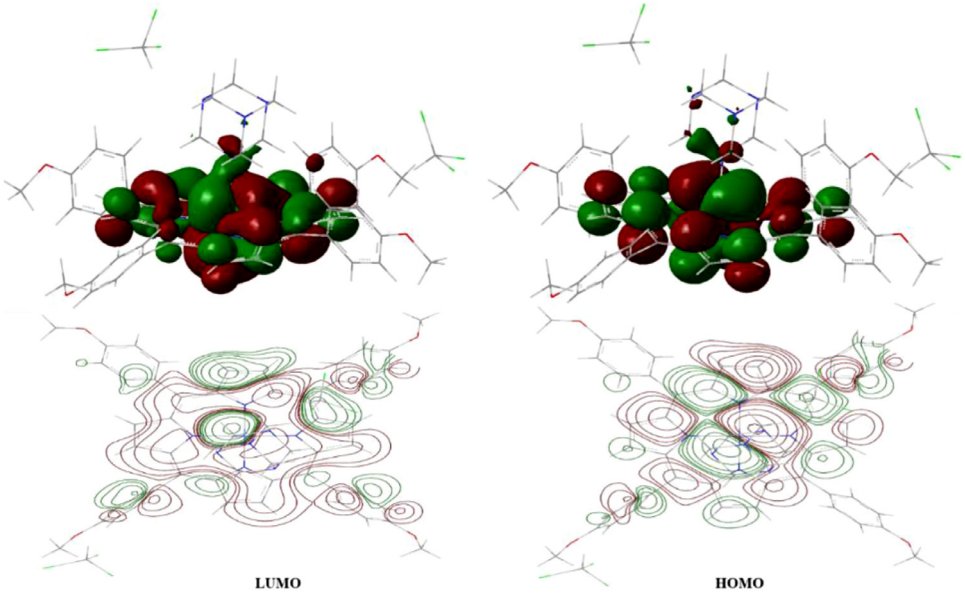

Fig. 10. 3D surfaces and 2D contour maps showing the electron density distribution of HOMO and LUMO orbitals.

eV and the highest occupied molecular orbital (HOMO) energy is -0.744 eV. Hence, computed HOMO-LUMO energy gap is found to be 2.106 eV (Fig. 11) and it seems in good agreement with corresponding experimental value 2.09 eV, obtained from UV-visible spectrum. On the basis of frontier orbitals energies, the different global reactivity descriptors such as chemical potential (μ), global hardness (η), and global softness (S) and global electrophilicity index (ω) are determined using Eqs. **(1) - (4)** as follows:

$$\mu = \frac{1}{2}(E_{LUMO} + E_{HOMO}) = 0.309\ eV \quad (1)$$

$$\eta = \frac{1}{2}(E_{LUMO} - E_{HOMO}) = 1.053\ eV \quad (2)$$

$$S = \frac{1}{2\eta} = 0.474\ eV \quad (3)$$

$$\omega = \frac{\mu^2}{2\eta} = 0.022\ eV \quad (4)$$

It is noted that for any two reactants, electrons flow from high to low chemical potential. The chemical hardness (η) and softness (S) of a molecule is a good indication of the chemical stability of the molecule. η is a direct measure of the electrophilic stability of a molecule, while S provides a measure of its electrophilic reactivity. A molecule with a high value of ω shows great propensity for attracting electrons from a generic donor molecule. Consequently, these results indicate low excitation energies for many of the excited states, low kinetic stability, and a high chemical softness for our studied complex. This also reveals that **(I)** can behaves as semiconductor material.

3.8. Adsorption kinetic

Fig. 12 represents the adsorption capacities (q_t) and the decolorization yields ($R\%$) of the vat yellow 1 dye in the presence of the H_2TMPP free base porphyrin and complex (**I**) as a function of time under the following experimental conditions: room temperature, Co = 25 mg.L^{-1} (of the vat dye) at pH = 6. The adsorbent capac-

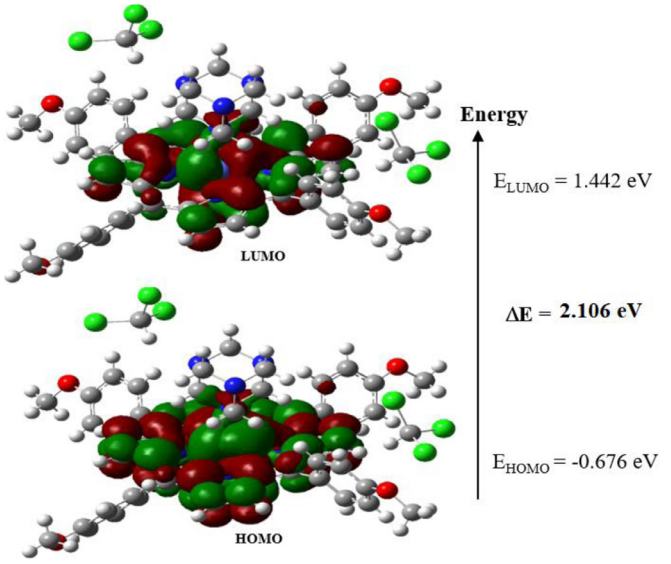

Fig. 11. HOMO–LUMO gap energy computed at UB3LYP/6-311+G(d,p)/SDD level of theory.

ity (q_t) is given by the relationship: q_t (mg.g^{-1}) = (C_o - C_t).(V/m) where C_o and C_t are the dye concentration before and after the adsorption, respectively. V is the volume of the dye used and m is the mass of the adsorbent. The q_t values are 3.5 and 3.1 mg.g^{-1}, respectively. By using the relationship (A_o – A_t)/A_ox100 (A_o and A_t are the absorption at t = 0 and at the t instant), the color removal yield values of H_2TMPP and (**I**) are 14% and 12.4%, respectively. We noticed that the adsorbent capacity and adsorption efficiency values of the free base porphyrin are slightly higher than those of [Co^{II}(TMPP)(HMTA)] (**I**) which could be related to the pyrrole hydrogen atoms in H_2TMPP leading to hydrogen bond type with the heteroatoms of the vat yellow dye molecues [83].

The fitting of the kinetic data of "H_2TMPP - vat yellow dye" and "complex **(I)** - vat yellow dye" systems was made using four kinetic models; namely the pseudo first order kinetic model, the pseudo second order kinetic model, the intraparticle diffusion model and the Elovich model [84]. In Fig. 13 are depicted the experimental data of the adsorption of vat yellow 1 dye on H_2TMPP and complex **(I)** while the data were fitted using the four kinetic models and the results are collected in Table S3.

Based on the regression coefficient R^2 (Table S3), the experimental results are better fitted using the pseudo second order model for both H_2TMPP and [Co^{II}(TMPP)(HMTA)] species with R^2 values of 0.99 and 0.97, respectively. The second order model equation that we used is as follows:

$$\frac{t}{q_t} = \frac{1}{(q_e{}^2 * k_2)} + \frac{t}{q_e}$$

where, q_t and q_e represent the amounts of the adsorbent adsorbed at time t and at equilibrium respectively, while k_2 is the rate constant for the pseudo second order model (g.mg^{-1}.min^{-1}). The values of k_2 and q_{cal} were calculated, for each one of the two porphyrinic compounds, from the slope and the intersection of the corresponding plot, respectively.

3.9. Degradation of the vat yellow 1 dye

The ability of the cobaltous-HMTA complex (**I**) to catalyze the degradation of the vat yellow dye was tested using an aqueous hydrogen peroxide solution and a photodegradation process using the solar light. In Fig. 14-a, are shown the curves C_t/C_o verses time (C_t and C_o are the concentration of the vat dye at the instants t and t = 0, respectively). The degradation yield ($R\%$) is given by the relation:

$$R(\%) = \left(1 - \frac{C_t}{C_o}\right).100.$$

By mixing only the vat yellow 1 dye and our Co(II) derivative (**I**), the $R\%$ value is 12.4%, after 120 mins of reaction. When we add an aqueous hydrogen peroxide solution (6 mg.L^{-1}) to this mixture, we noticed a large increase of the removal yield with a value of 72%, after 120 mins of reaction. This result could be ascribed to the important role of H_2O_2 which is activated by [Co^{II}(TMPP)(HMTA)] (**I**) complex [27]. Furthermore, when the same degradation reaction is made by using the solar light instead of the H_2O_2 oxidant reagent, the removal yield value is 63%, after 120 mins of reaction. Therefore, the photodegradation is considered an important method and also an environmental way to remove the vat yellow 1 dye, in presence of complex (**I**), mostly because only the solar light is used. where C_t and C_o being the vat yellow 1 dye concentration at times t and 0; t is the time of degradation and K_o is the first order rate constant. As shown in Fig. 14-b, when only the vat yellow dye and (**I**) are used, K_o value is 0.001 min^{-1} (with a correlation value R^2 of 0.74) which changes to 0.013 min^{-1} (R^2 = 0.99) in the presence of H_2O_2 solution and 0.008 min^{-1} (R^2 = 0.99) in the presence of a solar light.

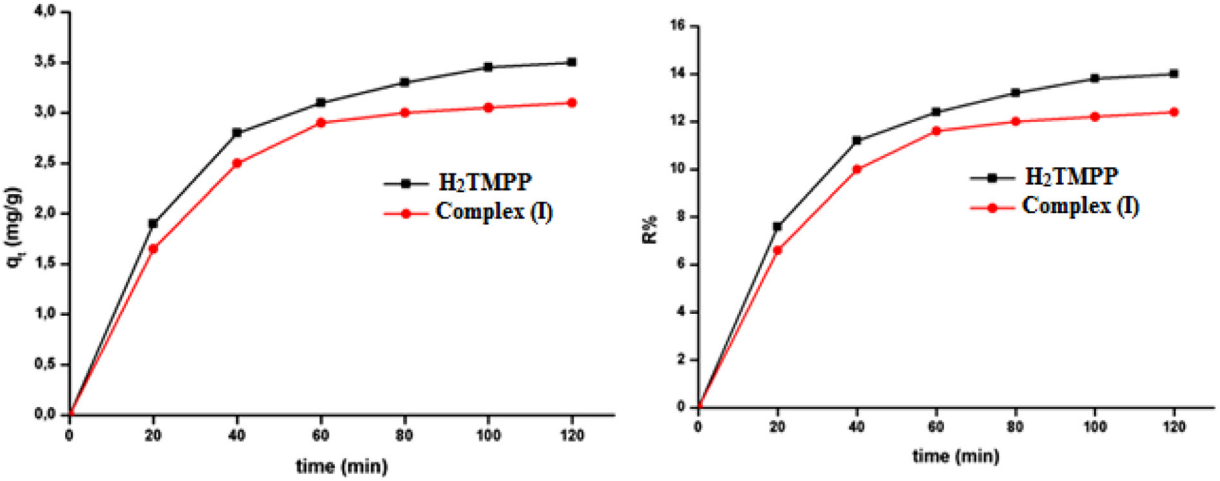

Fig. 12. Variation of the adsorption capacity (q_t) (left) and the removal yield ($R\%$) (right) vs. time for the vat yellow 1 dye using H_2TMPP and complex (**I**).

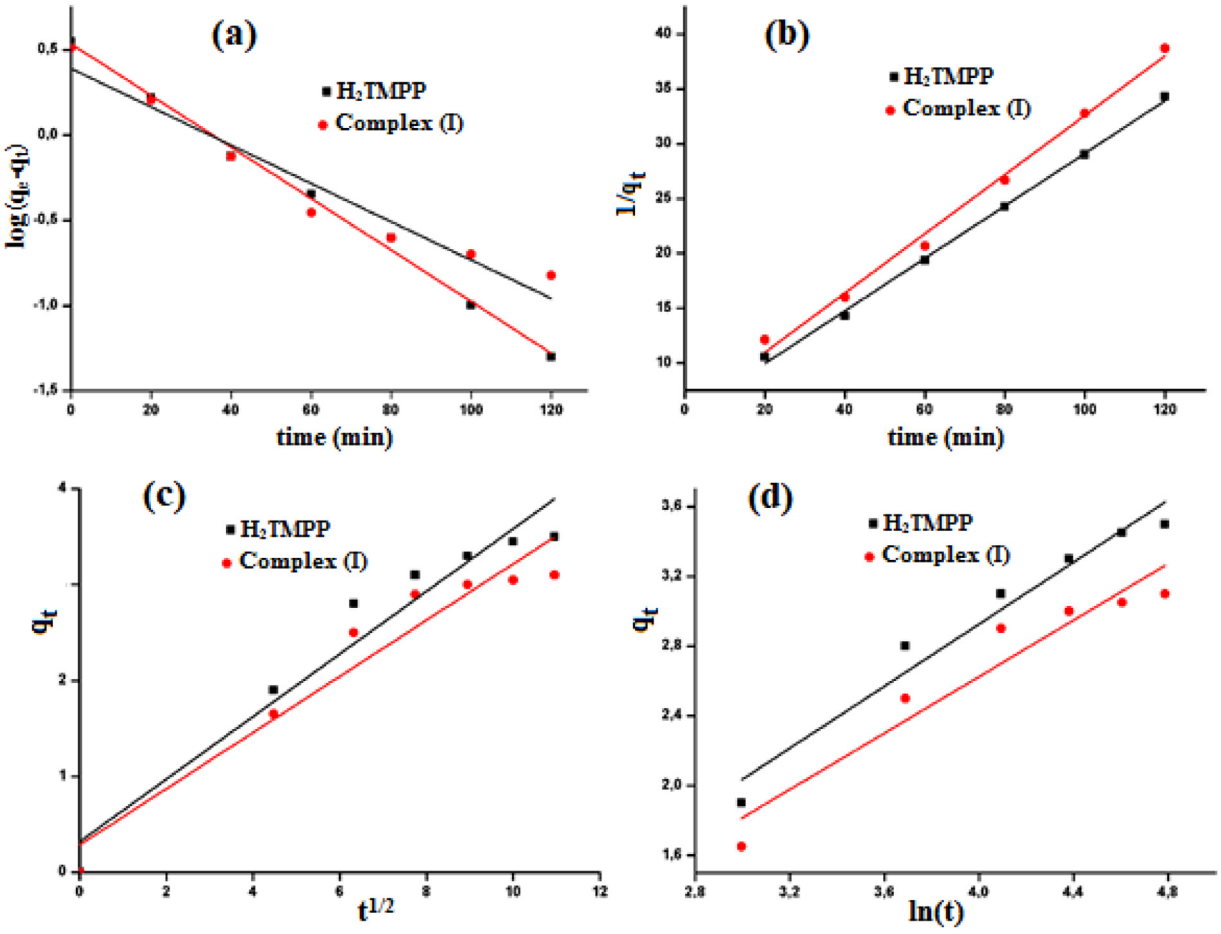

Fig. 13. Kinetic modeling for the adsorption of the vat yellow 1 dye in the presence of H_2TMPP and **(I). (a):** Pseudo first order model, **(b)**: Pseudo second order model, **(c):** Elovich model and **(d):** intra-particular diffusion model.

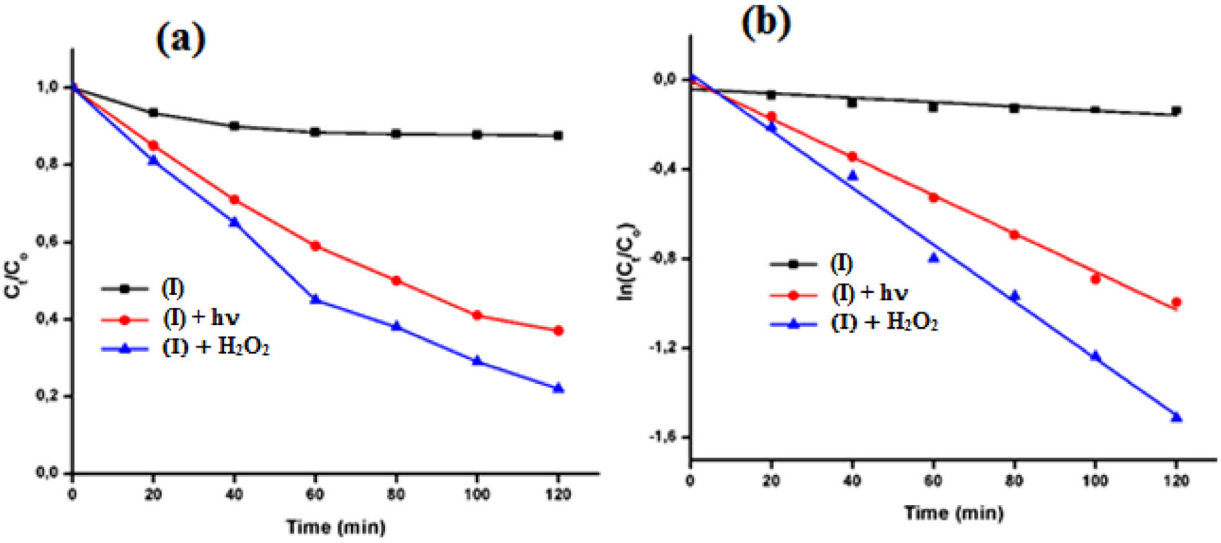

Fig. 14. (a): Variation of C_t/C_o as a function of time. **(b):** Variation of $In(C_t/C_o)$ as function of time. The lines represent the fitting data using the pseudo first order kinetic model.

3.10. Comparison of our procedure with other reported methods

The complete degradation of anthraquinone vat dyes such as the vat yellow 1 dye is difficult due the characteristic chemical stability of these species. Several degradation technics of vat yellow dyes are reported in the literature. This is the case of the biodegradation [85] and the filtration [86] methods. Recently, Atta-Eyison [87] reported the heterogeneous photocatalysis decomposition of the vat yellow 1 dye using zinc oxide photocatalyst in aqueous solution under UV and solar irradiation. The decomposition reaches 90% at 150 min of UV irradiation. Using our catalytic degradation method of the vat yellow 1 dye, the yield (72%) is smaller than

that of the photocatalytic method used by Atta-Eyison. Nevertheless, the encouraging obtained result using our cobaltous derivative (**I**) complex prompted us to use this compound in other methods of decomposition of this dye.

4. Conclusion

The reaction of an excess of hexamethylenetetramine (HMTA) with the *meso*-[tetra(*para*-methoxyphenyl)porphyrinato]cobalt(II) [Co^{II}(TMPP] starting material leads to the pentacoordinated [Co^{II}(TMPP)(HMTA)]$^{\bullet}$2$CHCl_3$ species (**I**) as confirmed by room temperature (RT) and low temperature (LT) X-ray molecular structures which indicate also that there is no structural change when the temperature is lowered. The UV-visible titration, ^{1}H NMR as well as the ESI and MALDI-TOF mass spectrometry show that in dichloromethane solvent, complex (**I**) is present as Co(II)-HMTA five-coordinated metalloporphyrin. The SQUID data indicated that at low temperature (below 220 K) complex (**I**) is a cobalt(II) low-spin porphyrin complex. Above this temperature, the magnetic properties show a gradual and incomplete spin crossover towards the high-spin state ($S = 3/2$). The cyclic voltammogram of (**I**), recorded in dichloromethane, shows a one-electron reversible oxidation wave of the $E_{1/2}$[(Co(II)/Co(III)] half-potential value shifted to positive potential indicating an easy oxidation of the Co(II) for our derivative. The crystal packing of (**I**) is stabilized by weak C–H•••O and C–H•••N hydrogen bonds and C—H···Cg and C–Cl···Cg intermolecular interactions involving the phenyl and pyrrole ring centroids. Furthermore, Base on Hirshfeld topology analyses all possible intermolecular interactions occurring in the crystal structure have been quantified. Frontier molecular orbitals energies and global reactivity descriptors reveal the high chemical reactivity and a low kinetic stability of the title complex. The adsorption efficiency of vat yellow 1 dye on H_2TMPP and complex (**I**) revealed that the free base porphyrin presents higher adsorption efficiency than the cobaltous HMTA derivative and that the pseudo second order kinetic model is the most appropriate to describe the adsorption process. The [Co^{II}(TMPP)(HMTA)] coordination compound was also tested as catalyst for the vat yellow dye 1 degradation using at first a hydrogen peroxide solution and then by photodegradation under solar light. Even though the first method affords a better removal yield ($R\% = 72\%$), the photodegradation degradation way, using the solar light, presents definitely a good removal yield of 63% since this technic is less expensive and environmentally friendly.

Statement of contributions of authors

Author 1
Name: Soumaya Nasri
Contribution: Synthesis of the species reported in the manuscript (corresponding author)
Author 2
Name: Melek Hajji
Contribution: Theoretical calculations
Author 3
Name: Mouhieddinne Guergueb
Contribution: UV-visible titration
Author 4
Name: Selma Dhifaoui
Contribution: Catalytic degradation of the dye
Author 5
Name: Valérie Marvaud
Contribution: SQUID investigation
Author 6
Name: Frédérique Loiseau
Contribution: Fluorescence study
Author 7
Name: Florian Molton
Contribution: Cyclic voltammetry investigation
Author 8
Name: Thierry Roisnel
Contribution: X-ray molecular structure data collection
Author 9
Name: Taha Guerfel
Contribution: DFT calculations
Author 10
Name: Habib Nasri
Contribution: Writing the manuscript

Declaration of Competing Interest

There are no conflicts to declare.

Acknowledgements

The authors gratefully acknowledge the Ministry of Higher Education and Scientific Research of Tunisia for financial support. The authors extend their appreciation to the deanship of Scientific Research at Majmaah University, Saudi Arabia.

Supplementary materials

Supplementary material associated with this article can be found, in the online version, at doi:10.1016/j.molstruc.2020.129676.

References

[1] J.M. Assour, J. Chem. Phys. 43 (1965) 2477–2489.
[2] F.A. Walker, J. Am. Chem. Soc. 92 (1970) 4235–2244.
[3] P.W. Lau, J. Inorg. nucl. Chem. 37 (1975) 2389–2398.
[4] L.A. Truxillo, D.G. Davis, Anal. Chem. 47 (1975) 2260–2267.
[5] F.A. Walker, J. Am. Chem. Soc. 95 (1973) 1154–1159.
[6] A. Shirazi, Goff, Inorg. Chem. 21 (1982) 3420–3425.
[7] F.A. Walker, J. Am. Chem. Soc. 95 (1973) 1150–1153.
[8] F.A. Walker, D. Beroiz, K.M. Kadish, J. Am. Chem. Soc. 98 (1976) 3484–3489.
[9] D.V. Stynes, C.Stynes H, J.A. Ibers, B.R. James, J. Am. Chem. Soc. 95 (1973) 1142–1149.
[10] J.A. Ibers, J. Am. Chem. Soc. 95 (1973) 1796–1801.
[11] Y. Belghish, A. Mansour, J.-C. Daran, H. Nasri, Open Journal of Inorganic Chemistry 2 (2012) 81–87.
[12] S. Zhu, X.X. Xu, J.A. Perman, X.P. Zhang, J. Am. Chem. Soc. 132 (2010) 12796–12799.
[13] S. Cheng, J. Wu, J. Bioelechem. 92 (2013) 22–26.
[14] S. Lin, C.S. Diercks, Y.-B. Zhang, N. Kornienko, E.M. Nichols, Y. Zhao, A.R. Paris, D. Kim, P. Yang, O.M. Yaghi, C.J. Chang, Science 349 (2015) 1208–1213.
[15] G. Karimipour, S. Kowkabi, A. Naghiha, Braz. Arch. Biol. Technol. 58 (2015) 431–442.
[16] M. Florescu, M. David, Sensors 17 (2017) 1–16.
[17] A. Colombelli, M.G. Manera, V. Borovkov, G. Giancanec, L. Valli, R. Rell, Sensors and Actuators B: Chemical 246 (2017) 1039–1048.
[18] M. Nango, T. Iwasaki, Y. Takeuchi, Y. Kurono, J. Tokuda, R. Oura, Langmuir 14 (1998) 3272–3278.
[19] G.R. Hodges, J.R.L. Smith, J. Oakes, J. Chem. Soc. Perkin Trans. 2 (1998) 617–627.
[20] T. Iwasaki, Y. Takeuchi, A. Kashiwada, M. Nango, Text. Res. J. 69 (1999) 956–960.
[21] D.S.L. Balan, R.T.R. Monteiro, J. Biotechnol. 89 (2001) 141–145.
[22] E. Makhado, S. Pandey, K. Desmond Modibane, M. Kang, M. Joseph Hato, Int. J. Biol. Macromol,
[23] , 162, 60-73.
[24] E. Gkaniatsou, C. Sicard, R. Ricoux, L. Benahmed, F. Bourdreux, Q. Zhang, C. Serre, J.-P. Mahy, N. Steunou, Angew. Chem. Int. Ed. 57 (2018) 16141–16146.
[25] S. Pandey, K. K. Mandari, J. Kim, M. Kang, E. F. Kankeu, in *Photocatalysts in Advanced Oxidation Processes for Wastewater Treatment*, 2020, 6, 167-196.
[26] R. Soury, M. Jabli, T.A. Saleh, W.S. Abdul-Hassan, E. Saint-Aman, F. Loiseau, C. Philouze, H. Nasri, RSC Advances 8 (2018) 20143–20156.
[27] M. Guergueb, J. Brahmi, S. Nasri, F.K.Aouadi Loiseau, V. Guerineau, S. Najmudin, H. Nasri, RSC Advances 10 (2020) 22712–22725.
[28] M. Guergueb, S. Nasri, J. Brahmi, F. Loiseau, F. Molton, T. Roisnel, V. Guerineau, I. Turowska-Tyrk, K. Aouadi, H. Nasri, RSC Adv 10 (2020) 6900–6918.
[29] A.D. Adler, F.R. Longo, J.D. Finarelli, J. Goldmacher, J. Assour, L.A.A. Korsakoff, J. Org. Chem. 32 (1967) 476–476.
[30] D. Toronto, F. Sarrazin, J. Pecaut, J.-C. Marchon, M. Shang, W.R. Scheidt, Inorg. Chem. 37 (1998) 526–531.
[31] A. Earnshaw, in: Introduction to Magnetochemistry, First ed., Academic Press, New York, London, 1968, pp. 1–4.

[32] A.D. Becke, J. Chem. Phys. 98 (1993) 5648–5652.
[33] M. Dolg, U. Wedig, H. Stoll, H. Preuss, J. Chem. Phys. 86 (1987) 866–872.
[34] K. Fukui, Science 218 (1982) 747–754.
[35] L. Padmaja, C. Ravikumar, D. Sajan, I.H. Joe, V.S. Jayakumar, G.R. Pettit, O.F. Nielsen, J. Raman Spectrosc. 40 (2009) 419–428.
[36] C. Ravikumar, C.I.H. Joe, V.S. Jayakumar, Chem. Phys. Lett. 460 (2008) 552–558.
[37] I. Fleming, Frontier orbitals and organic chemical reactions, John Wiley and Sons, New York, 1976.
[38] J.S. Griffith, L.E. Orgel, Rev. Chem. Soc. 11 (1957) 381–383.
[39] M.A. Spackman, D. Jayatilaka, D. CrystEngComm 11 (2009) 19–32.
[40] A.Y. Meyer, Chem. Soc. Rev. 15 (1986) 449–474.
[41] M. Hajji, N. Amiri, F. Ben Taheur, A. Bujacz, H. Nasri, T. Guerfel, Solid State Sci 10 (2020) 106117 https://doi.org/10.1016/j.solidstatesciences.2020.106117.
[42] S. Tetteh, Heliyon 5 (2019) e02125 5.
[43] Bruker, APEX2, SAINT-Plus and SADABS, Bruker AXS, Inc., Madison, Wisconsin, USA, 2014.
[44] A. Altomare, G. Casacarano, C. Giacovazzo, A. Guagliardi, M.C. Burla, G. Polidori, M. Camalli, J. Appl. Crystallogr. 27 (1994) 435–436.
[45] G.M. Sheldrick, Acta Crystallogr., Sect. C. 71 (2015) 3–8.
[46] A. Mansour, M. Zaied, S. Soliman, M. Othmani, Polyhedron 127 (2017) 496–504.
[47] N. Amiri, M. Hajji, F. Ben Taheur, S. Chevreux, T. Roisnel, G. Lemercier, H. Nasri, J. Solid State Chem. 258 (2018) 477–484.
[48] Q. Zeng, J. Lu, S. Xu, D. Wu, C. Liu, Y. Li, C. Wang, C. Bai, Lett. Org. Chem. 2 (2005) 424–427.
[49] A. Mansour, Y. Belghith, M.-S. Belkhiria, A.B. Bujacs, V. Guérineau, H. Nasri, J. Porphyrins Phthalocyanines. 17 (2013) 1094–1103.
[50] H. Sugimoto, N. Ueda, M. Mori, Bull. Chem. Soc. Jpn. 54 (1981) 3425–3432.
[51] M. Albrecht, M. Maji, C. Häusl, A. Monney, H. Müller-Bunz, Inorg. Chim. Acta. 380 (2012) 90–95.
[52] K. Yamamoto, Inorg. Chim. Acta 113 (1986) 181–186.
[53] Y. Terazono, B.O. Patrick, D.H. Dolphin, Inorg. Chim. Acta 346 (2003) 265–269.
[54] X.Q. Lin, B. Boisselier-Cocolios, K.M. Kadish, Inorg. Chem. 25 (1986) 3242–3248.
[55] V.V. Smirnov, E.K. Woller, S.G. DiMagno, Inorg. Chem. 37 (1998) 4971–4978.
[56] D.P. Rillema, C.M.C.M. Wicker, R.D. Morgan Jr, L.F. Barringer, L.A. Scism, J. Am. Chem. Soc. 104 (1982) 1276–1281.
[57] K.M. Kadish, L.A. Bottomley, D. Beroiz, Inorg. Chem. 17 (1978) 1124–1129.
[58] J. Li, C.B. Noll, A.G. Oliver, G. Ferraudi, A.G. Lappin, W.R. Scheidt, Inorg. Chem. 49 (2010) 2398–2406.
[59] J.R. Darwent, P. Douglas, A. Harriman, G. Porter, M.-C. Richoux, Coord. Chem. Rev. 44 (1982) 83–126.
[60] W.R. Scheidt, J. Am. Chem. Soc. 96 (1974) 84–89.
[61] V.P. Andreeva, P.S. Soboleva, D.O. Zaitsevb, L.A. Remizovac S. G. Tunina, Russ. J. Gen. Chem. 82 (2012) 1157–1166.
[62] W.R. Scheidt, J. Am. Chem. Soc. 96 (1974) 90–94.
[63] Y. Iimura, T. Sakurai, K. Yamamoto, Bull. Chem. Soc. Jpn. 61 (1988) 821–826.
[64] D.V. Konarev, S.S. Khasanov, G. Saito, R.L. Lyubovskaya, Y. Yoshida, A. Otsuka, Chem. Eur. J. 9 (2003) 3837–3848.
[65] B.F.O. Nascimento, M. Pineiro, A.M. d'A. R. Gonsalves, M.R. Silva, A.M. Beja, J.A. Paixão, J. Porphyrins Phthalocyanines 11 (2007) 77–84.
[66] Z.-S. Li, J.-S. Chai, Acta Cryst E63 (2007) m1533–m1535.
[67] W.R. Scheidt, Y. Lee, Struct. Bond. (Berlin) 64 (1987) 1–7.
[68] M. Vinodu, I. Goldberg, New J. Chem. 28 (2004) 1250–1254.
[69] K. Ezzayani, A. Ben Khelifa, E. Saint-Aman, F. Loiseau, H. Nasri, J. Mol. Struct. 1137 (2017) 412–418.
[70] H.-L. Zhu, S.-C. Shao, X.-Y. Qiu, L. Sun, L.S. Yang, J.-L. Ma, New Cryst.Struct. 218 (2003) 513–514.
[71] W.-L. Shang, Y. Bai, C.-Z. Ma, Z.-M. Li, Acta Crystallogr. Sect.E 64 (2008) m1184–m1185.
[72] P.-E. Werner, Cryst. Struct. Commun. 5 (1976) 873.
[73] Z. Liu, H. Xi, X. Sun, J. Zhu, K. Yu, Chin. J. Chem. Struc. Chem. 4 (2002) 355–358.
[74] J. Chakraborty, B. Samanta, G. Rosair, V. Gramlich, M.S. El Fallah, J. Ribas, T. Matsushita, S. Mitra, Polyhedron 25 (2006) 3006–3016.
[75] M. Č. Romanović, M.R. Milenković, A. Pevec, A.T. Iztok, V. Spasojević, S. Grubišić, D. Radanović, K. Anđelković, B. Čobeljić, Polyhedron 139 (2018) 142–147.
[76] K.M. Kadish, X.Q. Lin, B.C. Han, Inorg. Chem. 26 (1987) 4161–4167.
[77] K.M. Kadish, X.H. Mu, X. Q.Lin, Inorg. Chem. 27 (1988) 1489–1492.
[78] C. Paul-Roth, J. Rault-Berthelot, G. Simonneaux, C. Poriel, M. Abdalilah, J. Letessier, J. Electroanal. Chem. 597 (2006) 19–27.
[79] M.A. Spackman, J.J. McKinnon, CrystEngComm 4 (2002) 378–392.
[80] J.J. McKinnon, D. Jayatilaka, M.A. Spackman, Chem. Commun. 37 (2007) 3814–3816.
[81] M. J. Turner, J. J. McKinnon, S. K. Wolff, D. Grimwood, J. P. R. Spackman, D. Jayatilaka, M. A. Spackman, Three New Compounds Derived from Nitrofurantoin: X-Ray Structures and Hirshfeld Surface Analyses. CrystalExplorer17, 2017, University of Western Australia.
[82] D. Jayatilaka, D.J. Grimwood, A. Tonto, Computational Science – ICCS 4 (2003) 142–151.
[83] D. Jayatilaka, D. J. Grimwood, A. A. Lee, A System for Computational Chemistry, the University of Western Australia, Nedlands, Australia, 2005.
[84] S. Chowdhury, P. Das, Sep. Sci. Technol. 46 (2011) 1966–1976.
[85] C.T. Tovar, Jaraba, Ing. Univ. 19 (2015) 283–298.
[86] R. Yuan, S. Ramjaun, Z. Wang, J. Liu, Chem. Eng. J. 192 (2012) 171–178.
[87] D. Ratna, B.S. Padhi, J. Environ, Sci. Int. 3 (2012) 940–955.